Western Graduate&PostdoctoralStudies

Western University
Scholarship@Western

Electronic Thesis and Dissertation Repository

8-15-2018 2:00 PM

Functional CT Imaging for Myocardial Salvage in Acute Myocardial Infarction Management

Lisa Yun Jeong Hur, *The University of Western Ontario*

Supervisor: Drangova, Maria, *The University of Western Ontario*
Co-Supervisor: So, Aaron, *The University of Western Ontario*
A thesis submitted in partial fulfillment of the requirements for the Master of Science degree in Medical Biophysics
© Lisa Yun Jeong Hur 2018

Follow this and additional works at: https://ir.lib.uwo.ca/etd

Recommended Citation

Hur, Lisa Yun Jeong, "Functional CT Imaging for Myocardial Salvage in Acute Myocardial Infarction Management" (2018). *Electronic Thesis and Dissertation Repository*. 5538.
https://ir.lib.uwo.ca/etd/5538

This Dissertation/Thesis is brought to you for free and open access by Scholarship@Western. It has been accepted for inclusion in Electronic Thesis and Dissertation Repository by an authorized administrator of Scholarship@Western. For more information, please contact wlswadmin@uwo.ca.

Abstract

Hospitalization and revascularization treatment for patients with acute myocardial infarction (AMI) is an economic burden that can be minimized by identifying patients most likely to benefit. To this end, a non-invasive imaging technique to better characterize myocardial salvage may be helpful. In this thesis work, a functional CT technique is examined to assess at-risk, infarcted, and salvageable myocardial tissue. Data was acquired on a cohort of seven pigs with induced AMI during the acute and sub-acute phases post insult. The tracer kinetic model dependent CT images were validated against both T2-TIRM images and quantitative T1-maps acquired using MRI, as well as constant infusion CT images. Extravascular contrast distribution volume (ECDV) and myocardial perfusion (MP) parameters were used to characterize the injured myocardium. Derived ECDV and MP threshold for acute phase MI in seven pigs is 0.36 ml/g and 0.44 ml/min/g, respectively. Average MP in normal, at-risk and infarcted myocardium were 0.92 ± 0.27, 0.80 ± 0.19, 0.30 ± 0.08 ml/min/g, respectively. Average ECDV in normal, at-risk, and infarcted myocardium were 0.13 ± 0.08, 0.21 ± 0.07, 0.60 ± 0.12 ml/g, respectively. Significance was demonstrated in both MP and ECDV measurements between infarcted myocardium and myocardium at-risk, as well as between infarcted and normal myocardium ($p < 0.01$). Based on the area estimated using ECDV and MP, at-risk, infarcted, and salvageable myocardial tissue can be delineated.

Keywords

Acute myocardial infarction, CT Perfusion, myocardial edema, percutaneous coronary intervention, myocardial salvage, myocardium at-risk, infarct, myocardial perfusion, extravascular contrast distribution volume

Co-Authorship Statement

Chapter 2 is under preparation for submission to the Journal of the American College of Cardiology: Cardiovascular Imaging as a manuscript entitled: *"Functional CT Imaging to Identify Salvageable Myocardium for Acute Myocardial Infarction Management."* This manuscript is co-authored by Lisa Hur, Patrick Teefy, Gerald Wisenberg, Ting-Yim Lee, Maria Drangova, and Aaron So. As the first author of this manuscript, I have significantly contributed to the preparation of the manuscript for submission. I was responsible for: retrospective reconstruction of previously acquired CT raw data, data post-processing, and statistical analysis. I contributed to data interpretation and its clinical relevance and drafted the manuscript. Dr. Teefy, an interventional cardiologist, conducted the catheterization procedure, and was assisted by Dr. Wisenberg on the site of occlusion and the medications required to ensure survival of the animal during and after the interventional procedure. Dr. Lee provided the implemented software for analysis of our data and took part in the study design. Dr. Maria Drangova contributed to data analysis and interpretation. Dr. So contributed to the study design, acquisition of subject data, the development of the extended Johnson Wilson Lee tracer kinetic model for acute myocardial infarction, as well as data analysis and interpretation. Drs Drangova and So also contributed to manuscript revision.

To my grandfather…

Acknowledgments

This thesis work was accomplished with the generous help from numerous individuals. First, I would like to acknowledge my supervisors, Drs. Maria Drangova and Aaron So for their endless leadership, guidance, and support. I am grateful of the opportunity you have provided me at Western University. Your patience gave me the time to acknowledge my failures, and your expertise has helped me during the stumbles I could not resolve on my own. They have dedicated countless hours to perfect abstracts, posters, and oral presentations for various conferences such as Imaging Network of Ontario, London Health Research Day, Robarts Research Retreat and Radiological Society of North America (RSNA). Dr. Drangova, I cannot express how appreciative I am of the emotional support and friendship you have provided regardless of the time of day I visited your office. Dr. So has been very generous in funding me and giving me the privilege to travel to Chicago, United States to present my thesis work at the RSNA conference. I am truly grateful my supervisors were genuinely interested in bringing success to my academic work and ensuring I achieve my personal aspirations. I would also like to thank the members of my advisory committee, Dr. Chris Ellis and Dr. Ian Cunningham for providing feedback to my work and testing my knowledge.

I would like to thank Dr. Ting-Yim Lee, my “London dad”. Although you have many of your own graduate students, you made yourself available for valuable discussions and guidance. It was an honor to continue working with you at Western University. Your passion for research and ability to carry-on a diverse topic of research has truly inspired me since my undergraduate study.

My utmost gratitude is for Xiaogang Chen and the “Lee lab ladies”—Jennifer Hadway, Anne Leaist, Laura Morrison, Lise Desjardins. Xiaogang has programmed and debugged many of the softwares used for data analysis for this thesis work. For the Lee lab ladies, thank you for taking the time to teach me how to run the CT scanners, ensuring all experiments were carried out without a hiccup, and feeding us hungry students every Tuesday. Their dedication to the Lee lab has truly made London friendlier. I want to also thank the MR technologists, John Butler and Heather Biernaski, for your help imaging all the subjects used for this project. A special thanks to the other lab members: Feng Su, Danny

Yang, Raanan Marants, Kyle Burgers, Fiona Li, and Eric Wright. Thank you for your company and moral support, it has made my graduate student life memorable.

I want to thank my family; Mom, Dad and Justin. I know it was difficult—especially because we are the only family in Canada with no relatives, so you felt the need to keep us all together—but I thank you for letting me go. I was able to make my own choices, and when I fell, I was responsible for it without the need to blame you. Through every tears and desire to pack everything up, you told me to toughen up. Yet, you were all ready to come visit London when you felt I needed it. For that, I love you all so much.

To my dearest friends; April Chau, Charmainne Cruje, Jumin Lee, Dante Capaldi, Kevin Chung and Dickson Wong, I would not be where I am without you. April, you were always there to babysit my dog whenever I needed a break from work. You were always quick to reply to all my rants and our meme game remained strong since day one. Thank you. Charmainne and Jumin, you are the older sisters I never had. You were always there to support every decision I made—good or bad. To Dante and Kevin, your friendship has made my time over the past years memorable. You were the main source of my emotional support. Lastly, to Dickson. I will always be thankful for all that you have done and all that you continue to do for me and Byoli.

Table of Contents

Abstract i

Co-Authorship Statement ii

Acknowledgments iv

Table of Contents vi

List of Figures ix

List of Appendices xiii

List of Abbreviations xiv

CHAPTER 1 1

1 INTRODUCTION 1

1.1 Acute Myocardial Infarction: A consequence of coronary artery disease 1

1.1.1 Prevalence, mortality and economic burden of CAD 2

1.1.2 Management of acute coronary syndrome 3

1.1.3 Revascularization treatment 5

1.1.4 Progressive changes in myocardial perfusion post AMI 6

1.1.5 Pathophysiology of AMI and myocardial edema 6

1.2 Diagnostic imaging for early detection of AMI 10

1.2.1 Echocardiography 11

1.2.2 Cardiac magnetic resonance imaging 11

1.2.3 Single Photon Emission Computed Tomography 13

1.2.4 Coronary computed tomography 13

1.2.5 Dual energy computed tomography 14

1.2.6 Dynamic contrast enhanced computed tomography 15

1.3 Rationale and Clinical Translation 21

1.4 Purpose and Hypothesis 22

1.5 Thesis Overview 22

1.6 References 24

CHAPTER 2 31

2 Functional CT Imaging to Identify Salvageable Myocardium for Acute Myocardial Infarction Management 31

2.1 Introduction 31

2.2 Methods 32

2.2.1 Study design 32

2.2.2 Animal model 33

2.2.3 Data Acquisition 33

2.2.4 Data Analysis 35

2.3 Results 40

2.4 Discussion 47

2.5 Conclusion 49

2.6 Reference 50

CHAPTER 3 54

3 Conclusions and Future Work 54

3.1 Summary of Thesis Work 54

3.2 Study Limitations 55

3.3 Future Work 56

3.3.1 Monochromatic energy level to improve ECDV estimation 56

3.3.2 Validation of four-minute scan duration in estimating ECDV 58

3.3.3 Potential application of ECDV in sub-acute and chronic MI 59

3.3.4 Clinical Translation: triaging patients for revascularization treatment 63

3.4 References 64

Appendices 66

Reference 68

Curriculum Vitae 70

List of Figures

Figure 1-1 Categorization of STEMI, NSTEMI, and UA within ACS. Each subtype can be identified by ECG readings and blood sampling for cardiac biomarkers. 4

Figure 1-2 Normal myocyte in the absence of ischemic injury (left). Injured myocyte resulting from ischemic injury (right). Dash lines represent the loss of cell membrane integrity, making the surface of the cell membrane highly permeable 7

Figure 1-3 Fluid accumulation in the interstitial space of myocardium has two sources: blood vessel (capillary) and free water molecules of the cell via extracellular osmotic pressure forcing fluid to exit into the interstitial space. 8

Figure 1-4 The wave front phenomenon with initial ischemic and most affected area being the subendocardial region followed by subepicardial zone when a patient is left untreated. Myocardium at-risk (MAR) is the total area of tissue that is infarcted (irreversible injury) and can be salvaged (reversible injury). Assessment of MAR and infarcted myocardium will provide an estimate of how much tissue can be salvaged with intervention. 9

Figure 1-5 Ventilation suspension two seconds prior to a cardiac cycle and the scan performed at the diastolic phase of the cardiac cycle (at 75% R-R interval). 15

Figure 1-6 General time enhancement curve acquired during DCE-CT study of tissue (Q(t)) and arterial input ($C_a(t)$) used to derive functional parameters. Rapid scanning in the first phase is to ensure the wash-in of contrast agent is accurately measured. The second and third phase of the scan is at wider intervals to monitor the retention and slow wash out of contrast from the myocardium. 16

Figure 1-7 Flow-modified one-compartment Johnson and Wilson model of tracer kinetics. K_1 and k_2 are the influx and efflux rate constants, P = permeability coefficient, S = total surface area, V_v = volume of contrast in the vascular space, F= local blood flow, V_i = volume of contrast in the interstitial space, $C_a(t)$ = concentration of contrast in the input artery, $C_v(t)$ = concentration of contrast in the output vein. 18

Figure 1-8 Flow-modified two-compartment extended Johnson Wilson Lee model of tracer kinetics to account for the exchange of contrast in the addition cellular compartment. The dash line outlining the cellular compartment represents the loss of cell membrane integrity in acutely injured cardiomyocytes, increasing contrast permeability. K_1 = rate of influx from vascular compartment to interstitial compartment, k_2 = rate of efflux from interstitial to vascular compartment, k_3= rate of influx from interstitial to cellular compartment, k_4= rate of efflux from cellular to interstitial compartment. P = permeability coefficient, S = total surface area, F= local blood flow, V = volume of contrast, $C_a(t)$ = concentration of contrast in the input artery, $C_v(t)$ = concentration of contrast in the output vein. 20

Figure 2-1 ECDV map and MP map of the left ventricular myocardium of a sub-acute phase infarcted pig post ischemic insults corresponding to the dynamic CT image. A time enhancement curve (left) of the different myocardium region outlined on the ECDV and MP map. The time enhancement curve of the injured tissue (orange) shows higher elevation than the remote during the delayed phase of the scan (50-250s), due to the retention of contrast agent. 36

Figure 2-2 Difference image (right) generated by subtracting the pre-infusion image (center) from the post-infusion image (left). 37

Figure 2-3 Six segment horizontal long axis of the heart as defined by the AHA (30). These segments are supplied by the left anterior descending (LAD), right coronary (RCA), and the left circumflex (LCx) arteries. 38

Figure 2-4 (A) ECDV MAR depicted in the apical septal wall corresponds to the enhanced region of on the CI difference image (B) and T2 TIRM image (C). Injured myocardium is shown by the enhanced region (red arrow). The normal, uninjured mid-lateral wall (green arrow) is not enhanced. 40

Figure 2-5 (top) ECDV (ml/g) in infarcted and normal myocardium at acute and sub-acute stages post insult. (center) PC in infarcted and normal myocardium at acute and sub-acute stages post insult. (bottom) T2 TIRM signal intensity (a.u) in infarcted and normal myocardium at acute and sub-acute stages post insult. Error bars represent standard error

amongst the subjects (* denotes p < 0.05). Injured myocardium is represented by the apical-septal wall and the uninjured normal myocardium is represented by the mid-lateral wall. ... 41

Figure 2-6 (top) Difference of partition coefficient between MAR and remote normal tissue is shown for each of the seven pigs at the acute and sub-acute phases. (bottom) The same trends are seen for ECDV. (* denotes p < 0.05). 42

Figure 2-7 (top) Mean bias of percent area difference between CI and ECDV plotted on the y-axis. ECDV range plotted on the x-axis ECDV threshold of mean bias zero to delineate MAR is 0.36 ml/g for acute phase MVO and non-MVO cases. (bottom) Mean bias of percent area difference between CI and MP plotted on the y-axis. MP range plotted on the x-axis. MP threshold of mean bias zero to delineate infarct is 0.44 ml/min/g for acute phase MVO cases. Error bars represent the standard error..... 43

Figure 2-8 Mean MP (ml/min/g) and mean ECDV (ml/g) within different tissue states: infarct, at-risk, and normal, determined by MP and ECDV thresholds of 0.44 ml/min/g and 0.36 ml/g, respectively. Error bars represent standard error of forty-two slices from 7 pigs. (* denotes p < 0.05)..... 44

Figure 2-9 (left) contrast enhanced T1 map, CI difference image, MP, and ECDV maps of a single subject (center slice) with MVO and with minimal MVO (right) The colored regions correspond to the pixels flooded at specific thresholds. The ECDV scale is 0 to 1.2ml/g and MP scale from 0 to 5.0ml/min/g). The white arrows point to regions of MVO. 45

Figure 2-10 (top) subject with minimal MVO (bottom) subject with massive MVO. Yellow = infarcted myocardium estimated at MP <0.44ml/min/g. Pink = MAR in non-MVO cases and salvageable myocardium in MVO cases determined as ECDV >0.36ml/g. ECDV scale 0 to 1.2 ml/g and MP scale from 0 to 5.0 ml/min/g. 45

Figure 2-11 (left) MVO cases (n=5), comparing the area of infarct (MP), salvageable myocardium (ECDV), myocardium at risk (ECDV+MP) to the myocardium at risk area measured using CI. (right) non-MVO cases (n=2), comparing the area of infarct (MP), myocardium at risk (ECDV), salvageable myocardium (ECDV+MP) to the myocardium at risk area measured using CI. Error bars represent the standard error amongst each slice between subjects. ** p < 0.005, *** p < 0.001, **** p < 0.0001..... 46

Figure 3-1 ECDV functional maps generated at 70 keV and 50 keV of a single subject. Graphs on the right illustrate the normalized time enhancement curves of the injured apical septal wall (green) and normal mid-lateral myocardium (purple). 57

Figure 3-2 ECDV measurements (n=6) compared between images produced using 70 keV and 50 keV partial scan data. Error bars represent the standard error of the mean. (ns denotes no significance (p > 0.05)). 57

Figure 3-3 ECDV map of a two subjects (top and bottom row) at two different scan durations. ECDV map corresponding to the short scan duration utilizing three phases is shown on the left column and ECDV map corresponding to the long scan duration utilizing four phases is shown on the right column. Infarcted myocardium is denoted in orange and the normal (remote) myocardium is outlined in red. 59

Figure 3-4 Pathophysiology within infarcted myocardium at chronic MI. This figure depicts the development of extracellular matrix composed of high concentration of collagen fiber. 60

Figure 3-5 ECDV (left) and gadolinium enhanced MR (right) of a subject at acute MI and chronic MI. 61

Figure 3-6 CMR Gd enhanced T1 map (left). ECDV and perfusion functional map (top left and right, respectively). Iodine map at delayed phase and at peak contrast enhancement (bottom left and right, respectively). 62

Figure A-1 ECDV and MP maps of a subject using full scan and partial scan reconstruction. Graphs on the right illustrate the normalized time enhancement curves of the injured apical septal wall (green) and normal mid-lateral myocardium (purple). ECDV scale 0 to 1.2 ml/g and MP scale from 0 to 5.0 ml/min/g. 67

Figure A-2 ECDV (ml/g) of infarct and normal myocardium for each subject compared using full scan and partial scan reconstruction. (* denote p < 0.05, **** denote p < 0.0001). 67

List of Appendices

Appendix A: Quality of ECDV functional maps using full scan and partial scan retrospective reconstruction 66

Appendix B: Institution Research Ethics Board Approval 69

List of Abbreviations

ACC	American College of Cardiology
ACS	Acute Coronary Syndrome
AHA	American Heart Association
AMI	Acute Myocardial Infarction
ATP	Adenosine Triphosphate
CABG	Coronary Artery Bypass Grafting
CAD	Coronary Artery Disease
CCTA	Coronary Computed Tomography Angiography
CT	Computed Tomography
CVD	Cardiovascular Disease
DCE	Dynamic Contrast Enhanced
ECDV	Extravascular Contrast Distribution Volume
ECG	Electrocardiogram
JW	Johnson Wilson
JWL	Johnson Wilson Lee
LV	Left Ventricle
MAR	Myocardium At Risk
MP	Myocardial Perfusion
MRI	Magnetic Resonance Imaging
MVO	Microvascular Obstruction
NAD^+	Nicotinamide Adenine Dinucleotide
NSTEMI	Non ST-Elevation Myocardial Infarction
PCI	Percutaneous Coronary Intervention
STEMI	ST-Elevation Myocardial Infarction
SPECT	Single Photon Emission Computed Tomography
TIRM	Turbo Inversion Recovery Magnitude
T2-w	T2-weighted
UA	Unstable Angina

CHAPTER 1

1 INTRODUCTION

Acute myocardial infarction is the leading cause of death in Western countries. It remains a significant problem with great economic burden dedicated to patient management and treatment. Therefore, a guideline to triage patients for revascularization treatment will be of tremendous value for those involved in this process.

1.1 Acute Myocardial Infarction: A consequence of coronary artery disease

Coronary artery disease (CAD) occurs when one or more of the three main arteries supplying oxygen and nutrients to the heart muscle become damaged (1). Acute myocardial infarction (AMI) or heart attack is a consequence of CAD. It develops when regions of the heart become necrotic due to shortage of oxygen required for cellular metabolism, with prolonged ischemia (restricted blood supply). The majority of AMI events (9 out of 10) are caused by atherosclerosis, which is defined as the build-up of plaques that narrow or occlude a portion of the blood vessel (2). However, AMI is most often caused by an abrupt blockage of the vessel due to the rupturing of vulnerable plaque. This restricts the delivery of nutrients and causes ischemic injury that impairs the myocardium downstream of the occlusion site. Ischemic injury continues to advance until the affected artery is treated and blood supply is restored. If revascularization treatment is not pursued, perfusion to the myocardium will not be restored.

The severity of myocardial damage is dependent on the duration of unrelieved ischemia (3). Permanently irreversible damage (infarction) follows when the occlusion remains unresolved. Dense fibrous scar tissue takes the place of infarcted myocardium over time, and cardiac function becomes impaired. Symptoms of AMI are highly variable among the patient population. Common symptoms include chest and upper body discomfort, sweat, nausea, shortness of breath, and light-headedness. Some studies correlate the occurrence of AMI to time of day, with a greater incidence during the early morning hours as a

response to increased heart rate, blood pressure, and cardiac output in comparison to the later hours of the day (4). The symptoms listed above are common amongst many disease types. Hence, diagnosis and treatment planning remain ambiguous with clinical symptoms alone.

The aim of chapter one is to present the global burden of heart disease. It will define the group of patients who are most likely in need of further functional tests for conclusive diagnosis, and revascularization treatment guidance. Furthermore, the imaging techniques that are currently available and practiced in clinic for the assessment of AMI will be discussed; as well as the clinical implications of the novel functional CT technique described in chapter two, with the potential to triage patients for revascularization treatment.

1.1.1 Prevalence, mortality and economic burden of CAD

Diseases of the heart are the leading cause of death in the United States with 27.6 million diagnosed Americans (5,6). Within this population, approximately 610, 000 lives are lost to heart disease annually. In Canada, one in every twelve Canadian adults over the age of 21 is diagnosed with heart disease, and it is identified as the second leading cause of death with approximately fifty thousand individuals (7,8); this number represents twenty percent of the total number of deaths in 2013, as indicated by Statistics Canada. Heart disease is not prominent in one sex over another – it affects men and women equally. It is also agreed that the prevalence of the disease increases with age.

Heart disease makes up the majority of cardiovascular disease (CVD). Generally, CVD refers to different conditions that involve the loss of perfusion to different organ tissues that constitute the cardiovascular system. This includes CAD, heart failure, stroke, and hypertension. The American Heart Association and the American College of Cardiology's (AHA/ACC) 2018 statistical update suggests at least 130 million American adults are expected to be diagnosed with a form of CVD by the year 2035, by which time point the economic burden of CVD is estimated to reach $1.1 trillion per year (6). The majority of this cost is attributed to hospitalization and treatment of the diseased patients. Within the CVD population, 43.8% of deaths are associated with CAD, making it the

most common form of heart disease (9). In Canada, AMI caused by CAD is one of the top five reasons for inpatient hospitalization (10). Between the years 2016 and 2017, seventy thousand patients were hospitalized for an average of five days.

Currently, patients require comprehensive assessment upon arrival at the hospital. In certain cases, these patients are left untreated because they yield inconclusive results. This can potentially extend beyond the window of opportunity for revascularization treatment for patients who require immediate attention. To reduce the time between patient arrival at the hospital and transfer to the catherization lab, it is crucial to challenge current clinical guidelines in place for AMI patients, such that the most practical methods can be implemented to aid those in need of intervention, while limiting hospital expenses.

1.1.2 Management of acute coronary syndrome

Acute coronary syndrome (ACS) is an umbrella term that summarizes three conditions that result in a reduction of blood supply to the myocardium due to an abrupt blockage. Figure 1-1 provides an overview of the three ACS categories characterized based on electrocardiographic (ECG) recordings and blood work: ST segment elevation myocardial infarction (STEMI), non-ST segment elevation myocardial infarction (NSTEMI), and unstable angina (UA). When ACS is suspected, the 2014 AHA/ACC guidelines for management of patients with ACS suggest ECG tracings be acquired within 10 minute of hospital admission and monitored sporadically at 15 to 30-minute intervals to observe the dynamic changes in the presence of ischemic episodes (11).

Prolonged ST-segment elevation that deviates from previous baseline tracings is indicative of abrupt epicardial coronary artery occlusion(s) resulting in myocardial injury. Patients with STEMI are those with complete occlusions. These patients are unstable and urgently require revascularization treatment (11-13).

On the other hand, ACS patients who show no elevation of the ST segment require further testing before they can be classified into NSTEMI and UA. The ST-segment in this group of patients is not as prominent or distinct because the occlusion is partial or temporary. Blood tests are typically performed to determine the concentration of cardiac

biomarkers, such as troponin. Cardiac troponin is expressed exclusively in the heart and is effective in differentiating UA and NSTEMI. Levels of troponin T and troponin I are sensitive and specific indicators of myocardial damage that transpires with AMI (14,15); the greater the concentration of troponin T and I, the greater the volume of myocardial necrosis. For patients suspected of NSTEMI or UA, both the ECG and troponin levels are monitored at baseline (arrival) and throughout hospitalization, as changes in biomarker concentration can provide an understanding of the degree of myocardial impairment. Change of twenty percent or more from baseline troponin level are considered a significant increase. Patients presenting this change are classified as NSTEMI.

The third subcategory of interest comprises the patients with UA. Patients with UA have symptoms of severe, repeated chest pain that can potentially progress to myocardial infarction when left untreated. As UA patients have not experienced a heart attack or ischemia, troponin levels remain relatively stable over time—change less than 3 standard deviation between successive measurements—yielding inconclusive results.

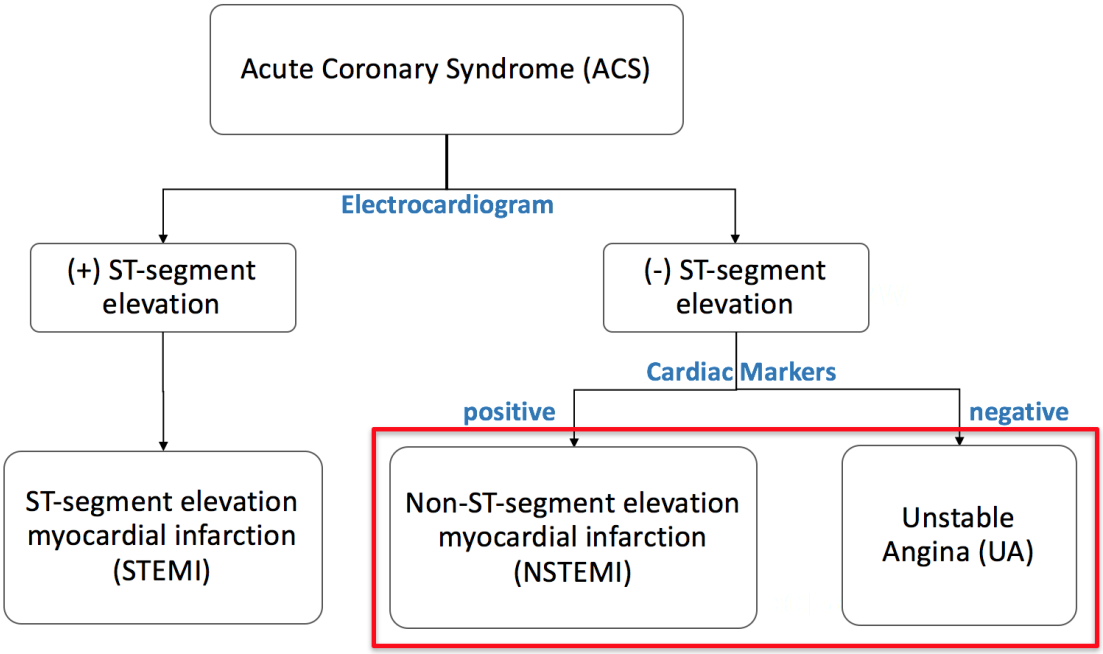

Figure 1-1 Categorization of STEMI, NSTEMI, and UA within ACS. Each subtype can be identified by ECG readings and blood sampling for cardiac biomarkers.

Because the combination of ECG tracings and troponin-level measurements yield inconclusive results, an additional non-invasive functional test is required to facilitate optimal patient management. This is especially important as statistics indicate two percent of patients discharged after presenting with asymptomatic serial ECG, biomarker, patient history, are later diagnosed with MI with greater risk of mortality (16,17). For these patients suspected of future episodes of MI, a non-invasive imaging technique may prove to be an advantageous diagnostic tool that can further characterize ischemically injured tissue to triage patients for revascularization treatment.

1.1.3 Revascularization treatment

When diagnosed with AMI, patients undergo revascularization via percutaneous coronary intervention (PCI, formerly known as coronary angioplasty). PCI is the primary non-surgical choice of treatment for AMI patients. This treatment requires cardiac catheterization, where a balloon catheter is advanced through the arm or groin, and guided to the region of occlusion by fluoroscopy. For structure support and guidance through the anatomical vessel, the balloon is placed within a metal stent. The balloon is inflated once the catheter traverses the stenosis to allow revascularization by compressing the plaque mass to the walls of the artery. When blood supply is restored in the myocardium in a timely manner, revascularization treatment is deemed successful and can prevent irreversible damage.

PCI is the preferred treatment for STEMI patients who present at the hospital within 2 hours post symptom onset (18). For best clinical outcome, PCI treatment should be performed within 120 minutes of diagnosis (19,20). In general, as in stroke studies, time delay or ischemic time is shown to be directly proportional to infarct size (21). Consequently, the left ventricular function (a measure of global cardiac function) become inversely proportional to time to revascularization in AMI (3,21,22).

Coronary artery bypass grafting surgery (CABG) is an invasive form of revascularization treatment, which is the most common open-heart surgery for NSTEMI-AMI patients. Briefly, a healthy artery or vein harvested from elsewhere in the body is grafted to bypass the blocked coronary artery thereby providing a new pathway for blood to access the

myocardium. Although PCI is a reference procedure for revascularization, previous clinical trials indicate CABG as the main standard of care for patients with complex disease when multiple vessels are occluded (23).

1.1.4 Progressive changes in myocardial perfusion post AMI

Coronary blood flow is directly proportional to the oxygen requirement or consumption of the heart. When the heart is stressed (e.g. exercise), the heart demands greater concentration of oxygen, compensated by more coronary blood flow. With partial occlusion of the artery, minimal oxygen is delivered through the occluded artery to meet the energy required by the heart to maintain function. In STEMI subjects with a complete occlusion, perfusion to the downstream muscles of the heart is completely lost in the coronary artery responsible for nutrient delivery. The muscle's alternative source of oxygen supply is dependent on the development of collateral vessels, which also has an upper limit. Collateral vessels can compensate the loss of coronary blood flow, but its ability to maintain high demands of oxygen is determined by the advancement of the collateral vessels of the subject. During the progression of AMI and the formation of a complete occlusion, myocardial perfusion is lost with time. In addition, with greater regions affected by MI there are greater degrees of microvascular obstruction (MVO) or damage. The delivery of blood through the microvasculature is absent in tissue with MVO.

1.1.5 Pathophysiology of AMI and myocardial edema

As discussed in section 1.1, AMI is caused by the blockage of an artery that supplies blood to the heart. MI is the death of cardiomyocytes after extended oxygen deprivation or ischemia. Infarcted myocardium cannot be salvaged because the adverse effects of ischemic injury are detrimental. In contrast, myocardium at risk (MAR) that surround the infarcted myocardium is not yet necrotic and can be salvaged when reperfused promptly. Myocardial edema occurs in regions of MAR in the event of ischemia; however, edema further extends in injured myocardium with revascularization after acute MI event. Edema is a physiological response of interest for this project as it targets the patient with partial or temporary stenosis with experienced ischemia and reperfusion. Following

occlusion, the loss of blood flow downstream results in limited delivery of oxygen to the tissue. Oxygen is an important reactant that the body requires to undergo a metabolic process for the production of adenosine triphosphate (ATP), a major energy source powering all other cellular processes in the human body. This metabolic process is referred to as cellular respiration, where the body uses stored sugar molecules of glucose and the available intake of oxygen to produce energy rich ATP (13,24-26).

ATP plays an important role in regulating the influx of water between the interstitial and cellular space. The ATP dependent sodium-potassium (Na^+/K^+) pump regulates the concentration of sodium and potassium inside and outside of the cell. For every three sodium ions extruding from the cell, two potassium ions enter the cell through the Na^+/K^+ pump. In the absence of oxygen, the concentration of ATP is reduced because the cell is unable to undergo cellular respiration. As a result, the ATP-dependent Na^+/K^+ pump becomes dysfunctional and leaky, allowing water to diffuse into the cell during the transportation of sodium ions (Figure 1-2) (25,26).

In normal myocardium, eighty percent of the myocardium is composed of water. Of this water, 78% are water molecules that are tightly bound to proteins and other

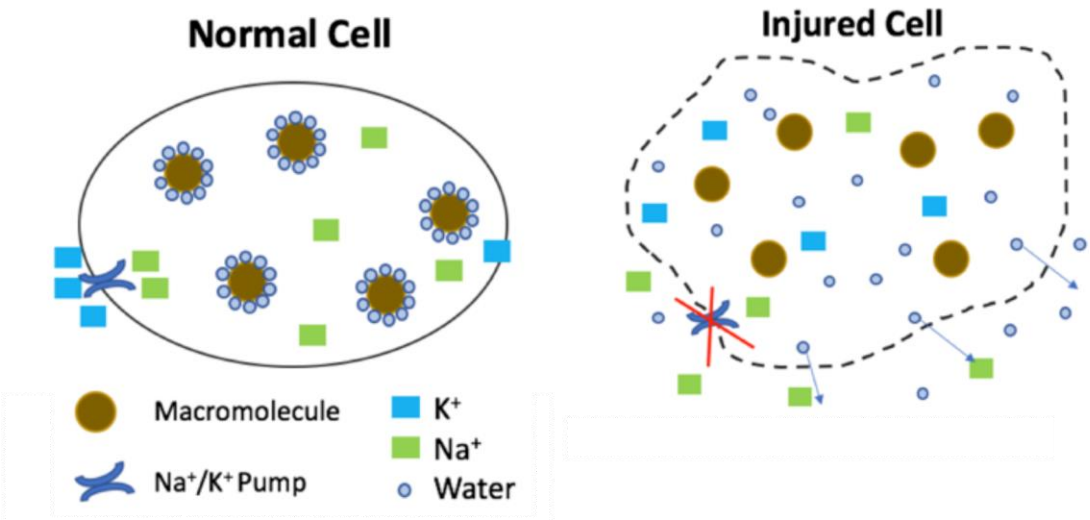

Figure 1-2 Normal myocyte in the absence of ischemic injury (left). Injured myocyte resulting from ischemic injury (right). Dash lines represent the loss of cell membrane integrity, making the surface of the cell membrane highly permeable

macromolecules (e.g. ribonucleic acid) within the myocyte. In oxygen deficient circumstances, the cell can alternatively depend on anaerobic respiration to produce a weaker source of energy, nicotinamide adenine dinucleotide (NAD^+). NAD^+ plays an important role in energy metabolism when oxygen is not readily available in the body system during environmental stress. Unfortunately, anaerobic respiration can only be effective for a short duration, when tissues are deprived of oxygen and a 'plan b' is required to maintain homeostasis. With prolonged occlusion where the supply of oxygen is insufficient relative to the tissue demand, anaerobic respiration can have detrimental effects on a molecular level.

A byproduct of anaerobic respiration is lactate. The sudden demand for anaerobic respiration increases the concentration of lactate in the cell, forcing the intracellular environment to be acidic. With abrupt decrease in pH, the proteins and macromolecules that bind to the water molecules undergo a conformational change, which releases the water molecules allowing localization throughout the intracellular space.

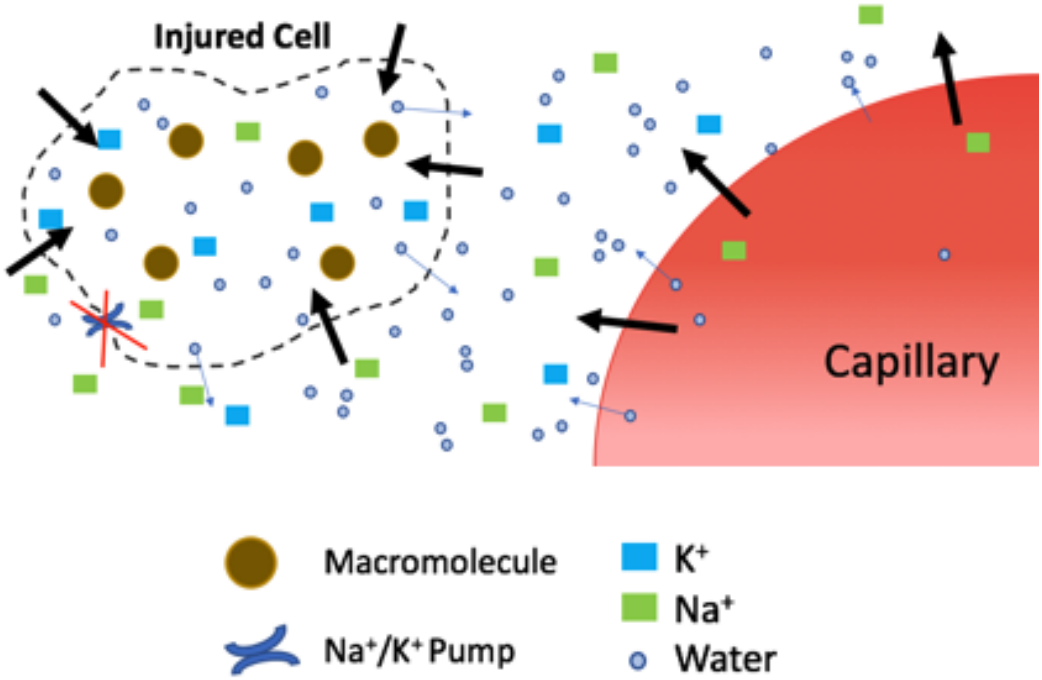

Figure 1-3 Fluid accumulation in the interstitial space of myocardium has two sources: blood vessel (capillary) and free water molecules of the cell via extracellular osmotic pressure forcing fluid to exit into the interstitial space.

Free water molecules in combination with the Na^+/K^+ pump malfunction are the main cause of cellular edema – the abnormal accumulation of water in a tissue – in the myocardium post AMI. It is important to note that edema in the myocardium takes place not only in the intracellular space but also in the interstitial space of the tissue.

Fluid accumulation in the interstitial space has two sources (Figure 1-3). The main source of water is the blood vessel. Edema is the aftermath of an inflammation response to stress, a precursor of Na^+/K^+ pump dysfunction. Like the Na^+/K^+ pump of a myocyte, Na^+/K^+ pumps are present around the cell membranes of endothelial cells that line the interior surface of the blood vessels. With ischemia, capillary membranes become semi-permeable due to the damage of endothelial cells. This means that following AMI, the endothelial cells undergo apoptosis, no longer able to guard the blood vessel from allowing the entrance and evacuation of unwanted materials. The capillary membrane becomes leaky, allowing fluid exchange between the vascular and interstitial space.

In addition to the leakiness of the blood vessels, the second source of edema in the interstitial space is the osmotic pressure gradient between the intracellular and extracellular space, forcing fluid to diffuse out of the edematous myocytes into its neighboring interstitial compartment (Figure 1-3).

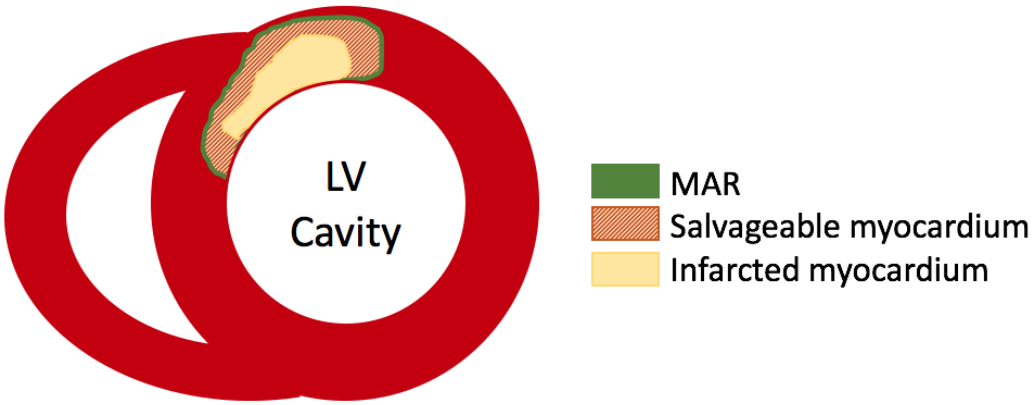

Figure 1-4 The wave front phenomenon with initial ischemic and most affected area being the subendocardial region followed by subepicardial zone when a patient is left untreated. Myocardium at-risk (MAR) is the total area of tissue that is infarcted (irreversible injury) and can be salvaged (reversible injury). Assessment of MAR and infarcted myocardium will provide an estimate of how much tissue can be salvaged with intervention.

Previous animal studies have shown that myocardial infarction follows a ‘wave front phenomenon’, where the subendocardial regions of the heart are most affected by ischemia and are first to become infarcted (27). Followed by the subendocardial regions is the subepicardial layer or the extended borders of the myocardium at risk (MAR) (Figure 1-4). Common characteristics of infarcted myocardium are the presence of myofibrillar contraction bands, damaged mitochondria (either swollen or ruptured), microvascular obstruction, and haemorrhage (27-29). The duration of unrelieved ischemia will influence the presence and continuance of ischemic/reperfusion injury. Comprehensive assessment of the injured tissue prior to proceeding with treatment is necessary to reason how much tissue is at risk and infarcted to estimate how much can be salvaged.

1.2 Diagnostic imaging for early detection of AMI

As stated in section 1.1.2, a non-invasive imaging technique may prove useful in tissue characterization for NSTEMI and UA patients with inconclusive results during the primary examinations performed upon arrival at the emergency department. Diagnostic imaging techniques take advantage of the cascade of physiological events that occur during hypoperfusion and reperfusion, to evaluate myocardial tissue state. Three tissue states of interest are infarcted and salvageable tissue, which together represent at-risk myocardium. This section will briefly describe the most commonly used imaging techniques for cardiac tissue evaluation as well as techniques to measure cardiac function. The following imaging techniques are used to evaluate CAD in both acute and chronic stages of MI. Not all of these techniques are routinely practiced for diagnosis of AMI (the focus of this thesis work). Echocardiography, single photon emission computed tomography (SPECT), magnetic resonance imaging (MRI), and x-ray computed tomography (CT) are common modalities for cardiac imaging. The preference of one imaging method over another is based on the specific information that the user wants to acquire. Three types of assessments are of importance: anatomical, mechanical, and functional. The purpose of an anatomical assessment in AMI is to examine the degree of lumen narrowing. Mechanical assessment can provide wall-motion abnormality information. The most direct assessment of tissue state (quantity of reversible tissue

relative to necrotic tissue) is by acquiring functional data. In the following section, the most prominent imaging modalities, and their role in assessing AMI will be discussed briefly.

1.2.1 Echocardiography

Echocardiography is a noninvasive imaging tool that is available at the bedside to visualize myocardial wall function during an ischemic process. Two-dimensional (2D) images are produced by the use of ultrasound for anatomical assessment, as well as myocardial function. Although echocardiography is not commonly used in diagnosing patients with AMI, echocardiography is a staple in clinical cardiology. In patients suspected of AMI, this imaging tool can locate abnormalities in wall motion (for example, myocardial stunning) and myocardial thickness. Echocardiography can also be used as a monitoring tool at the bedside to locate mechanical complications after MI event, to determine if a patient needs further treatment.

To improve contrast between ventricle and myocardium, technologist can choose to intravenously administer the patient with microsphere contrast agents. Echocardiographic contrast agents approved and used in clinic are Optison and Definity which are perflutren protein type A and perflutren lipid microspheres, respectively. Contrast echocardiography is useful it that it can also provide perfusion information in real time. Previous studies have proven the use of contrast echocardiography pre- and post- revascularization to assess the area at risk, in addition to infarct size (30). Overall, echocardiography of the heart is a practical approach to estimate global cardiac function of a patient; but a major limitation of this imaging technique worth mentioning is its high variance in image quality between operators.

1.2.2 Cardiac magnetic resonance imaging

MRI is used to investigate CAD in both acute and chronic MI. In diseases, such as stroke and AMI, MRI has been used to characterize tissue state with sufficient spatial resolution and excellent soft tissue contrast. In this section, two MRI techniques: gadolinium enhanced T1-mapping and T2-weighted (T2-w) imaging used to image myocardial viability will be discussed, with respect to its application for MI.

1.2.2.1 Post gadolinium enhanced T1-mapping

Gadolinium enhanced T1 mapping has been used for tissue characterization and assessment of myocardial viability (31,32). As the name suggests, it requires the administration of exogenous extracellular contrast agents to improve sensitivity. Gadolinium-DTPA (diethylenetriamine penta-acetic acid) is a Food and Drug Administration (FDA) approved contrast agent used in MR imaging, and is used to shorten the T1 spin-lattice relaxation time. Gd-DTPA accumulates in injured myocardium as a result of increased permeability in the interstitial and cellular space after AMI. Therefore, injured myocardium with retention of Gd-DTPA will appear hypoenhanced in gadolinium enhanced T1-maps; and can be delineated as MAR.

A limitation of gadolinium-enhanced imaging is the introduction of exogenous contrast agent to the body. Although it is a tracer amount of contrast, with the assumption that it takes no part in any physiological processes, it becomes problematic in patients subjected to renal failure. In patients with poor kidney function, gadolinium will retain in the body and cannot be cleared. This is a potential risk factor to consider in patients with history of kidney disease.

1.2.2.2 T2-weighted imaging

T2-weighted cardiac magnetic resonance imaging is sensitive to free water molecules in tissue. In AMI, it is useful in direct assessment of tissue edema (a marker of myocardium at risk of further infarction) (33). With this imaging technique, fluid filled regions of the tissue appear hyperenhanced relative to remote normal myocardium. It is a useful tool in delineating MAR in acute stages of MI, when myocardial edema is most prominent. MRI scientists have demonstrated the reduction in fluid over time after investigation of patients with MI at acute and chronic stages after ischemic insult (34).

T1-mapping to detect infarct and T2-w imaging to delineate MAR is shown to improve diagnostic accuracy in identifying tissue with reversible injury (24). Although this technique is practiced in the clinic, it is not practical in emergency settings since the MRI scanner is not accessible in most hospitals around the clock, and requires highly trained operators.

1.2.3 Single Photon Emission Computed Tomography

SPECT imaging is frequently used in clinic to assess myocardial perfusion for the evaluation of CAD. It is a nuclear medicine tomographic imaging technique which uses gamma rays and a gamma camera. A radioactive tracer – typically containing Technitium-99m or Fluorine-18 – is injected into the patient and the scanner detects gamma rays that are emitted by the tracer within the body. SPECT imaging is commonly combined with stress testing in patients with angina symptoms to reveal hemodynamic information prior to revascularization (37). This allows for comparison of myocardial perfusion measurements in myocardium at stress and myocardium at rest. The significant change in myocardial perfusion between stress and rest provide information on the degree of myocardial damage. Limitations of SPECT imaging is its sensitivity and radiation dose of approximately 4.5 mSv; which is higher than DCE-CT (3 mSv).

1.2.4 Coronary computed tomography

CT scanners have become one of the most available diagnostic and screening tools available in the hospital around the clock over the past decade. Their use has become more prominent with the ability to acquire axial and helical diagnostic images within seconds, facilitating patient throughput. Recent advances in CT technology have enabled the acquisition of high-resolution three-dimensional coronary angiograms in time periods shorter than fifteen minutes, including preparation time.

Coronary computed tomography angiography (CCTA) uses x-ray beams and exogenous contrast agents, such as iodine, at high tube current for anatomical assessment with great accuracy. The greatest advantage of CCTA is its ability to detect the site of stenosis and the degree of lumen narrowing at the site of interest. It is time efficient and noninvasive, while remaining an effective diagnostic approach (35). However, although CCTA is highly sensitive to the localization of the occlusion by imaging the distribution of contrast agent in the blood vessel and identifying the hypoenhanced region (site of occlusion where iodine cannot enter), it is not useful in evaluating the haemodynamic influence of the stenosis on the downstream myocardium. In other words, CCTA is not a tissue viability test and can only identify the presence of stenosis. Multicenter studies have

praised its ability to detect occlusion sites but have criticized its high negative predictive value with regards to assessing physiological ischemia (36,37).

To triage AMI patients for revascularization treatment, tissue viability (i.e. how much tissue can potentially be salvaged) is of interest. To do so, functional physiological parameters must be considered (38). For example, studies have emphasized perfusion measurements that can be obtained in conjunction with CCTA for improved evaluation of CAD severity, as 50% of stenosis located using CCTA alone is a poor predictor of ischemic injury (39,40).

1.2.5 Dual energy computed tomography

Spectral imaging or dual energy CT is a type of CT protocol that utilizes two different energy spectra (typically, 80 kVp and 140 kVp for clinical application). The main advantage of dual energy CT is its ability to decompose different anatomical features (i.e. differentiating bone, water, and blood vessels) (41). Material of unknown composition can be represented as a ratio of previously determined elements. Typically, the reference elemental composition of known value is water and iodine (exogenous extracellular CT contrast agent); and an unknown material would be identified as the ratio of water and iodine concentration.

A research topic of interest in MI to study the chronic stages post MI is the use of ‘iodine mapping’ to detect scar tissue (42). Iodine mapping is a static image acquired at peak enhancement of contrast in the tissue to quantify the amount of iodine concentration within a single pixel of the acquired image. Like MRI, CT requires the intravenous injection of exogenous iodine contrast agents, which is retained in the extracellular space of injured tissue. With basic knowledge of water and iodine density, iodine mapping can make use of material decomposition to quantify the ratio of iodine to water concentration within a single pixel to detect injured tissue and perfusion defects (43).The accumulation of contrast in the injured myocardium is the consequence of myocardium remodeling at the chronic stages of MI due to the dense fibrotic tissue content in the extracellular space. The myocardium region where scar and fibrosis are present would appear hyperenhanced with greater accumulation of iodine.

An additional advantage of dual energy CT is its ability to reduce artifacts such as beam-hardening effects (38). Beam hardening occurs as a result of greater attenuation of low energy x-ray beams than higher energy x-ray beams. The average x-ray after the beam passes the material will be higher due to this, i.e. hardening of the beam. This artifact can be corrected during image reconstruction by producing a virtual monochromatic image at a single energy (38,44).

1.2.6 Dynamic contrast enhanced computed tomography

Dynamic contrast enhanced (DCE) – CT is a functional imaging technique where a patient is injected with contrast and the enhancement of contrast in the organ of interest is monitored over time. During a dynamic imaging session of the heart, prospective ECG-gating is used to acquire a set of scan images at the same diastolic phase of the cardiac cycle (Figure 1-5). It provides functional information on the hemodynamics of the myocardium that cannot be acquired from a standard anatomical CT (45). Previously, DCE-CT images of the heart were acquired with retrospective ECG-gating technique, where the subjects were scanned during the whole cardiac cycle. Images were reconstructed retrospectively at a single cardiac cycle. With the advancement of prospective ECG-gating where a single scan is acquired at a specific phase of the cardiac cycle, the effective dose of radiation to the patient has been reduced from 12 mSv to 3mSv.

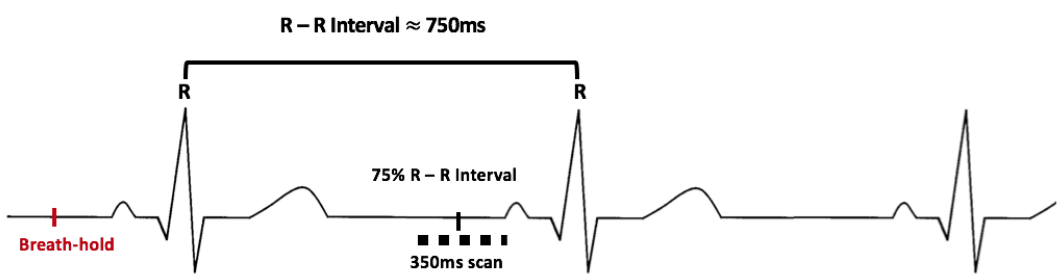

Figure 1-5 Ventilation suspension two seconds prior to a cardiac cycle and the scan performed at the diastolic phase of the cardiac cycle (at 75% R-R interval).

DCE-CT can be achieved using either a single energy or a dual energy CT to obtain quantitative functional data. Single energy DCE-CT requires advanced post image processing methods to correct for beam hardening effect. As mentioned in section 1.2.4, dual energy CT may have an advantage over single energy CT; for example, beam hardening correction and material decomposition.

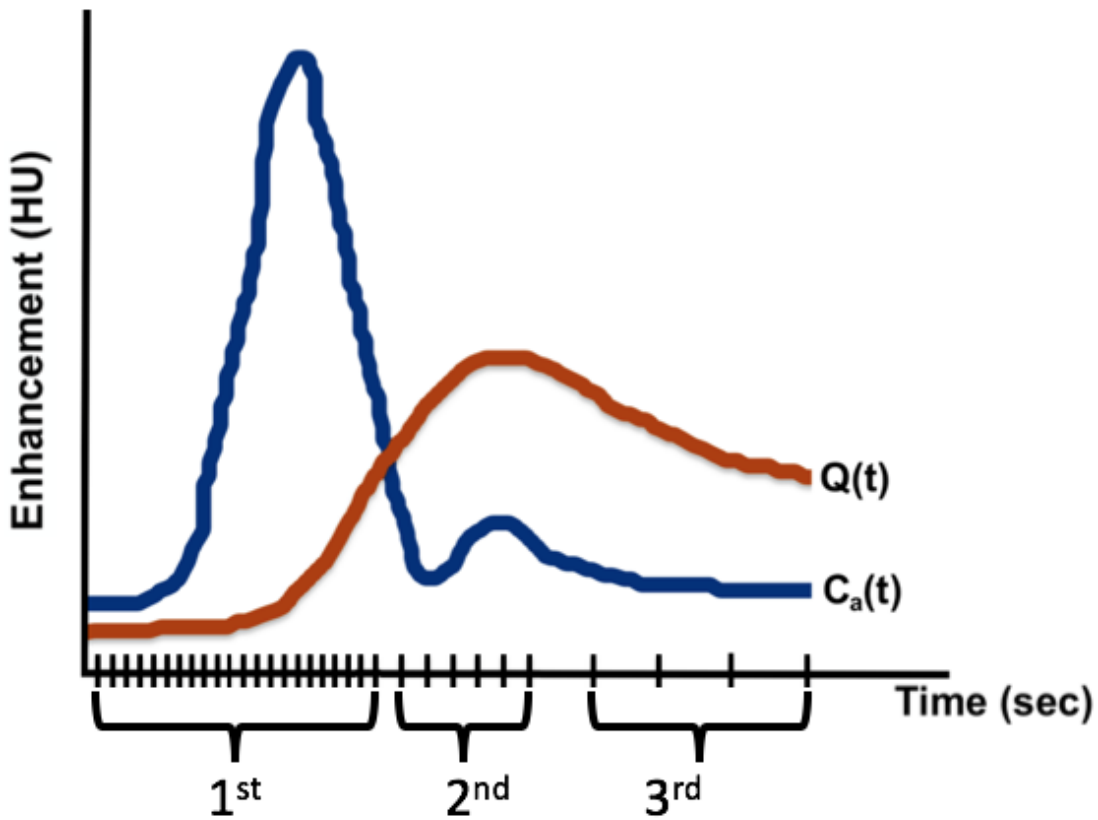

Figure 1-6 General time enhancement curve acquired during DCE-CT study of tissue (Q(t)) and arterial input ($C_a(t)$) used to derive functional parameters. Rapid scanning in the first phase is to ensure the wash-in of contrast agent is accurately measured. The second and third phase of the scan is at wider intervals to monitor the retention and slow wash out of contrast from the myocardium.

A contrast-enhanced image of an organ of interest is not enough to yield functional information. Tracer kinetic modeling for dynamic CT has been developed and used extensively in the evaluation of tissue hemodynamics. A tracer kinetic model must be applied to the time enhancement curve (in Hounsfield unit, HU) of the tissue and artery to

derive functional parameters such as perfusion (blood flow), blood volume, and mean transit time (Figure 1-6). This will be further discussed in section 1.2.6

1.2.6.1 Johnson Wilson Lee Model

Our lab has pioneered the Johnson Wilson Lee (JWL) capillary-tissue kinetic model to facilitate quantitative measurement of tissue perfusion from a single bolus injection of contrast medium and dynamic imaging session (44, 46). It has been applied to measure myocardial perfusion in pigs with reperfused acute myocardial infarction and in patients with known or suspected coronary artery disease (44). The JWL model describes the kinetic behaviour of contrast medium in a single capillary transit in a realistic manner: Firstly, it assumes that the concentration of contrast in the vascular space (capillaries) is spatially non-uniform and has a concentration gradient from the arterial inlet to the venous outlet. This assumption accounts for the exchange of contrast medium between the vascular and interstitial spaces through passive diffusion during its first-pass circulation. Secondly, it assumes that the contrast concentration gradient in the radial direction within the vascular space is negligible compared to that in the axial direction (from arterial to venous ends), because the flow rate in the axial direction is much greater than that in the radial direction within the vascular space. Thirdly, the interstitium is assumed to be a compartment, in which the contrast residues in the interstitium is well mixed and the contrast concentration in the interstitial space is homogenous. This assumption holds true because the capillaries in tissue are oriented randomly, hence, contrast can enter the interstitial space in all directions which justified the assumption of uniform mixture of contrast in this compartment. Furthermore, the rate of contrast movement in the interstitium is much slower compared to the flow rate in the vasculature.

The distribution of contrast medium within the myocardium is governed by two processes: (1) the wash-in and wash-out of contrast in and out of the vascular space via perfusion; (2) Passive diffusion of contrast between the vascular and the interstitial space through the permeable capillary endothelium. The bi-directional exchange of contrast between the vascular and interstitial spaces is governed by rate constants K_1 and k_2.

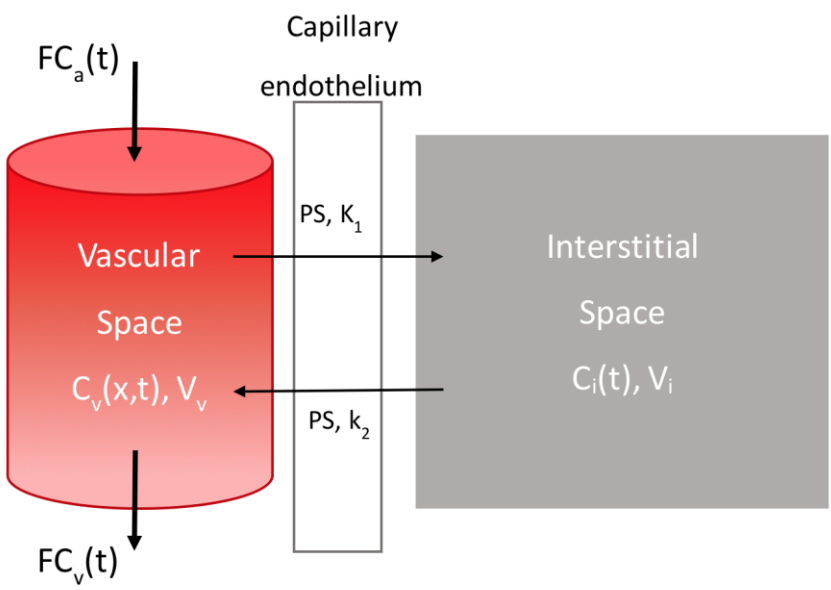

Figure 1-7 Flow-modified one-compartment Johnson and Wilson model of tracer kinetics. K_1 and k_2 are the influx and efflux rate constants, P = permeability coefficient, S = total surface area, V_v = volume of contrast in the vascular space, F= local blood flow, V_i = volume of contrast in the interstitial space, $C_a(t)$ = concentration of contrast in the input artery, $C_v(t)$ = concentration of contrast in the output vein.

The dynamic CT images acquired after a bolus injection of contrast can measure the tissue and arterial time-enhancement curve (TEC). Together with tissue blood flow, K_1 and k_2 can be estimated from the measured TECs using the JWL model. The tissue and arterial TEC have the following relationship:

$$\begin{aligned} Q(t) &= F \cdot [C_a(t) \otimes R(t)] \\ &= C_a(t) \otimes [F \cdot R(t)] \\ &= C_a(t) \otimes R_F(t) \end{aligned} \qquad \textbf{Eq. 1-1}$$

where Q(t) is the tissue TEC, F is the blood flow in tissue, $C_a(t)$ is the arterial TEC, $\otimes$ is the convolution operator, R(t) is the impulse residue function (IRF), and $R_F(t)$ is the flow-modified IRF. The IRF is the theoretical delta function that describes the tissue response to instantaneous delivery of contrast medium at the arterial inlet of the tissue. The height of IRF is unity. The flow-modified IRF has the following mathematical forms:

$$R_F(t) = \begin{cases} 0 & 0 \leq t < T_0 \\ F & T_0 \leq t < T_0 + W \\ F \cdot E \cdot e^{-\frac{F \cdot E}{V_i}(t-W)} & t > T_0 + W \end{cases} \qquad \textbf{Eq. 1-2}$$

where T_o is the contrast arrival time, W is the minimum transit time and V_i is the volume in the interstitial space. At time less than T_o, no contrast is delivered in the tissue and hence $R_F(t)$ remains zero. When contrast is delivered at the arterial inlet at T_o, $R_F(t)$ becomes F and remains as F for the time less than the minimum transit time, during which the contrast remains in the tissue. At time greater than W, a fraction of contrast is washed out at the venous end, and $R_F(t)$ is equal to the product of flow and extraction fraction (E) and an exponential term that describes the gradual decrease of contrast concentration in the tissue over time.

1.2.6.2 Extended Johnson Wilson Lee Model

CT contrast medium is an extracellular agent and metabolically inert, and does not distribute in tissue cells under normal condition. In the setting of acute myocardial infarction where the cell membrane integrity in injured myocardium is altered, CT contrast may gain access into the cellular space which may lead to a prolonged accumulation (47-51). To account for the kinetics behaviour of contrast in acutely injured myocardium, the JWL kinetic model is extended to simultaneously measure myocardial perfusion (MP) and extravascular contrast distribution volume (ECDV) (Figure 1-8). The latter parameter has a unit of mL per gram of tissue.

k_1 to k_2 in equation 1-3 are the rate constants describing the diffusion of contrast from the vascular space to the interstitial space, and vice versa; k_3 and k_4 are the rate constants that describe the diffusion of contrast from the interstitial space to cellular space, and vice versa.

The $R_F(t)$ has the following forms governed by the extended JWL model:

$$R_F(t) = \begin{cases} F & T_0 \le t < T_0 + W \\ F \cdot E & t = T_0 + W \\ G \cdot e^{-\alpha(t-w-T_0)} + H \cdot e^{-\beta(t-w-T_0)} & t > T_0 + W \end{cases}$$

$$G = K_1 \frac{k_3 + k_4 - \alpha}{\beta - \alpha} \quad \text{and} \quad H = K_1 \frac{\beta - k_3 - k_4}{\beta - \alpha}$$

$$\alpha = \frac{(k_2 + k_3 + k_4) - \sqrt{(k_2 + k_3 + k_4)^2 - 4k_2k_4}}{2} \qquad \textbf{Eq. 1-3}$$

$$\beta = \frac{(k_2 + k_3 + k_4) + \sqrt{(k_2 + k_3 + k_4)^2 - 4k_2k_4}}{2}$$

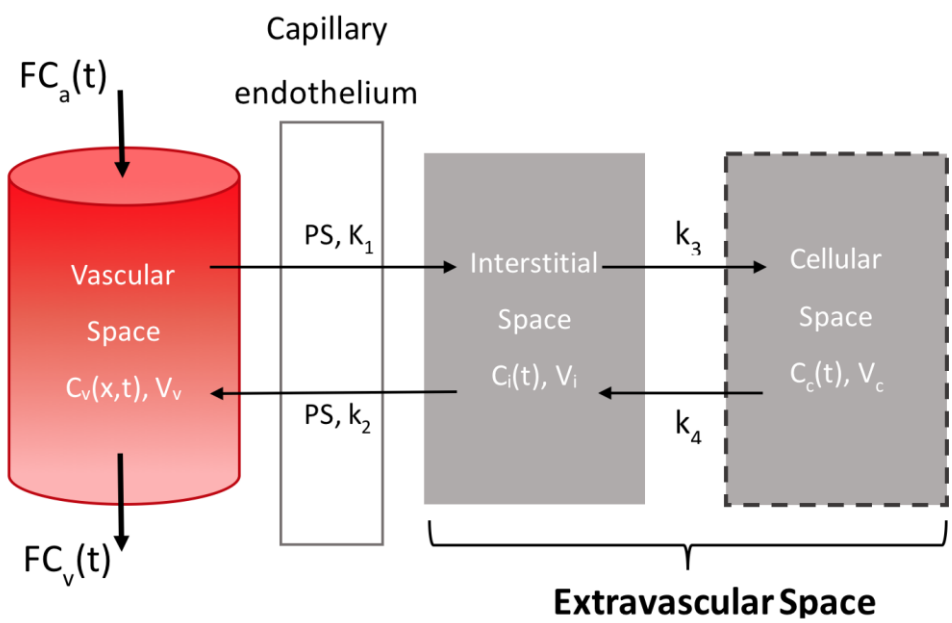

Figure 1-8 Flow-modified two-compartment extended Johnson Wilson Lee model of tracer kinetics to account for the exchange of contrast in the addition cellular compartment. The dash line outlining the cellular compartment represents the loss of cell membrane integrity in acutely injured cardiomyocytes, increasing contrast permeability. K_1 = rate of influx from vascular compartment to interstitial compartment, k_2 = rate of efflux from interstitial to vascular compartment, k_3= rate of influx from interstitial to cellular compartment, k_4= rate of efflux from cellular to interstitial compartment. P = permeability coefficient, S = total surface area, F= local blood flow, V = volume of contrast, $C_a(t)$ = concentration of contrast in the input artery, $C_v(t)$ = concentration of contrast in the output vein.

For time between T_o and $T_o + W$, the form of $R_F(t)$ described by the extended JWL model is identical to that described by the JWL model. The difference occurs at the time greater than $T_o + W$, where the gradual washout of contrast in the tissue is given by dual exponential terms in the extended JWL model to account for the involvement in both the interstitial and cellular compartments.

In summary, ECDV in normal tissue ($ECDV_{normal}$) is equal to the volume of contrast in the interstitial compartment (V_i). ECDV in infarcted tissue ($ECDV_{infarct}$) is equal to the sum of the V_i and the volume in the cellular compartment (V_c). Thus, ECDV in infarcted tissue will be greater than in normal tissue:

$$ECDV_{normal} = V_i \; ;$$

$$ECDV_{infarct} = V_i + V_c \; ;$$

$$ECDV_{infarct} > ECDV_{normal} \; .$$

$$ECDV_{infarct} = V_i + V_c = \frac{G}{\alpha} + \frac{H}{\beta} \qquad \textbf{Eq. 1-4}$$

1.3 Rationale and Clinical Translation

AMI caused by partial or complete occlusion of one or more coronary arteries becomes an economic burden from the moment of admission to treatment and care, followed by re-hospitalization when required. Lack of blood flow and oxygen delivery are detrimental to the myocardium, causing edema in the injured myocardial tissue. Myocardial edema is a hallmark of the ischemic (hypo-perfused) myocardium that is at risk of irreversible injury (infarction), and can be assessed non-invasively with T2-w MRI. Imaging the at-risk myocardium would be useful to inform decision making related to interventional revascularization treatment, particularly for patients who do not receive treatment promptly after a temporary or partial occlusion due to lack of evidence of salvageable myocardium Specifically, these patients include NSTEMI and UA patients described in

section 1.1.2. However, MRI is typically not available in the emergency setting and is rarely used to assess patients with AMI.

On the other hand, DCE CT is a fast imaging technique and has the potential of being widely available at hospitals; with many scanners sited in emergency departments. Our group has developed a functional CT method for measuring the distribution volume of contrast agent in the extravascular space of the myocardium and hypothesized that ECDV, assessed by CT, can be a surrogate marker of myocardial edema in MAR.

1.4 Purpose and Hypothesis

The purpose of my thesis is to validate ECDV estimated using the functional CT technique and to determine quantitative thresholds of ECDV and MP that can be used in delineating the extent of salvageable myocardium. The hypothesis of my work is that salvageable myocardium can be identified in DCE-CT as tissue that demonstrates the presence of edema with depressed blood flow, while infarcted myocardium exhibits marginal to no blood flow within the edematous region.

1.5 Thesis Overview

The overall objective of this research project is to demonstrate the potential use of DCE-CT to delineate salvageable myocardium by simultaneous assessment of edema and myocardial perfusion in a single dynamic imaging session.

In chapter 2, I validated the ECDV metric quantified using the extended JWL tracer kinetic model against the model independent constant infusion CT imaging method. We wanted to ensure that the ECDV estimated using a tracer kinetic model is a true surrogate of myocardial edema in injured myocardium after ischemic injury. After confirming ECDV as a marker of edema, I derived ECDV and MP thresholds on the same subjects used for validation at acute phase post AMI to delineate area of MAR, infarcted myocardium, and salvageable myocardium. Lastly, I compared the areas measured using the functional CT metrics to the area measured using the standard constant infusion CT technique to identify salvageable myocardium.

Chapter 2 is in preparation for submission as a paper to the Journal of the American College of Cardiology: Cardiovascular Imaging entitled “Functional CT Imaging to Identify Salvageable Myocardium for Acute Myocardial Infarction Management”.

The last chapter (Chapter 3) summarizes the thesis results, discusses the limitations of the functional CT technique, and describe possible future work that will improve ECDV measurement. This thesis work will conclude by discussing the clinical translation of the functional CT technique.

1.6 References

1. Libby P, Theroux P. Pathophysiology of coronary artery disease. Circulation 2005;111:3481-8.

2. Ambrose JA, Singh M. Pathophysiology of coronary artery disease leading to acute coronary syndromes. F1000Prime Rep 2015;7:08.

3. De Luca G, Suryapranata H, Ottervanger JP, Antman EM. Time delay to treatment and mortality in primary angioplasty for acute myocardial infarction: every minute of delay counts. Circulation 2004;109:1223-5.

4. Durgan DJ, Pulinilkunnil T, Villegas-Montoya C et al. Short communication: ischemia/reperfusion tolerance is time-of-day-dependent: mediation by the cardiomyocyte circadian clock. Circ Res 2010;106:546-50.

5. Benjamin EJ, Blaha MJ, Chiuve SE et al. Heart Disease and Stroke Statistics-2017 Update: A Report From the American Heart Association. Circulation 2017;135:e146-e603.

6. Benjamin EJ, Virani SS, Callaway CW et al. Heart Disease and Stroke Statistics-2018 Update: A Report From the American Heart Association. Circulation 2018;137:e67-e492.

7. Statistics Canada. The ten leading causes of death, 2013. Ottawa (ON): Statistics Canada, 2015.

8. Public Health Agency of Canada. Heart Disease in Canada: Highlights from the Canadian chronic disease surveillance system. 2017.

9. Murphy SL, Xu J, Kochanek KD, Curtain SC, Arias E. Deaths: Final Data for 2015. National Vital Statistics Report 2017;66.

10. The Canadian Institute for Health Information (CIHI). Inpatient Hospitalizations, Surgeries, Newborns and Childborth Indicators, 2016-2017. 2018.

11. Amsterdam EA, Wenger NK, Brindis RG et al. 2014 AHA/ACC Guideline for the Management of Patients with Non-ST-Elevation Acute Coronary Syndromes: a report of the American College of Cardiology/American Heart Association Task Force on Practice Guidelines. J Am Coll Cardiol 2014;64:e139-e228.

12. Yiadom MY, Baugh CW, McWade CM et al. Performance of Emergency Department Screening Criteria for an Early ECG to Identify ST-Segment Elevation Myocardial Infarction. J Am Heart Assoc 2017;6:1-11.

13. Ibanez B, Heusch G, Ovize M, Van de Werf F. Evolving therapies for myocardial ischemia/reperfusion injury. J Am Coll Cardiol 2015;65:1454-71.

14. Mahajan VS, Jarolim P. How to interpret elevated cardiac troponin levels. Circulation 2011;124:2350-4.

15. Wetterstem N, Maisel A. Role of Cardiac Troponin Levels in Acute Heart Failure. Cardiac Failure Review 2015;1:102-106.

16. Farkouh M, Smars P, Reeder GS et al. A clinical trial of a chest-pain observation unit for patients with unstable angina. The New England Journal of Medicine 1998;339:1882-1888.

17. Tatum JL, Jesse RL, Kontos MC et al. Comprehensive Stratefy for the Evaluation and Triage of the Chest Pain Patient. Annals of Emergency Medicine: An International Journal 1996;29:116-125.

18. Bagai A, Dangas GD, Stone GW, Granger CB. Reperfusion strategies in acute coronary syndromes. Circ Res 2014;114:1918-28.

19. Ibanez B, James S, Agewall S et al. 2017 ESC Guidelines for the management of acute myocardial infarction in patients presenting with ST-segment elevation: The Task Force for the management of acute myocardial infarction in patients presenting with ST-segment elevation of the European Society of Cardiology (ESC). Eur Heart J 2018;39:119-177.

20. Steg PG, Juliard JM. Primary percutaneous coronary intervention in acute myocardial infarction: time, time, and time! Heart 2005;91:993-4.

21. Francone M, Bucciarelli-Ducci C, Carbone I et al. Impact of primary coronary angioplasty delay on myocardial salvage, infarct size, and microvascular damage in patients with ST-segment elevation myocardial infarction: insight from cardiovascular magnetic resonance. J Am Coll Cardiol 2009;54:2145-53.

22. Guerchicoff A, Brener SJ, Maehara A et al. Impact of delay to reperfusion on reperfusion success, infarct size, and clinical outcomes in patients with ST-segment elevation myocardial infarction: the INFUSE-AMI Trial (INFUSE-Anterior Myocardial Infarction). JACC Cardiovasc Interv 2014;7:733-40.

23. Mohr FW, Morice M-C, Kappetein AP et al. Coronary artery bypass graft surgery versus percutaneous coronary intervention in patients with three-vessel disease and left main coronary disease: 5-year follow-up of the randomised, clinical SYNTAX trial. The Lancet 2013;381:629-638.

24. Abdel-Aty H, Cocker M, Meek C, Tyberg JV, Friedrich MG. Edema as a very early marker for acute myocardial ischemia: a cardiovascular magnetic resonance study. J Am Coll Cardiol 2009;53:1194-201.

25. Friedrich MG. Myocardial edema--a new clinical entity? Nat Rev Cardiol 2010;7:292-6.

26. Garcia-Dorado D, Andres-Villarreal M, Ruiz-Meana M, Inserte J, Barba I. Myocardial edema: a translational view. J Mol Cell Cardiol 2012;52:931-9.

27. Reimer K, Lowe J, Rasmussen M, Jennings R. The Wavefront Phenomenon of Ischemic Cell Death 1. Mycardial Infarct Size vs Duration of Coronary Occlusion in Dogs. Circulation 1977;56:786-794.

28. Jennings RB. Historical perspective on the pathology of myocardial ischemia/reperfusion injury. Circ Res 2013;113:428-38.

29. Heusch G, Gersh BJ. The pathophysiology of acute myocardial infarction and strategies of protection beyond reperfusion: a continual challenge. Eur Heart J 2017;38:774-784.

30. Micari A, Belcik TA, Balcells EA et al. Improvement in microvascular reflow and reduction of infarct size with adenosine in patients undergoing primary coronary stenting. Am J Cardiol 2005;96:1410-5.

31. Taylor AJ, Salerno M, Dharmakumar R, Jerosch-Herold M. T1 Mapping: Basic Techniques and Clinical Applications. JACC Cardiovasc Imaging 2016;9:67-81.

32. Kammerlander AA, Marzluf BA, Zotter-Tufaro C et al. T1 Mapping by CMR Imaging: From Histological Validation to Clinical Implication. JACC Cardiovasc Imaging 2016;9:14-23.

33. Friedrich MG, Kim HW, Kim RJ. T2-weighted imaging to assess post-infarct myocardium at risk. JACC Cardiovasc Imaging 2011;4:1014-21.

34. Walls MC, Verhaert D, Min JK, Raman SV. Myocardial edema imaging in acute coronary syndromes. J Magn Reson Imaging 2011;34:1243-50.

35. Goldstein JA, Chinnaiyan KM, Abidov A et al. The CT-STAT (Coronary Computed Tomographic Angiography for Systematic Triage of Acute Chest Pain Patients to Treatment) trial. J Am Coll Cardiol 2011;58:1414-22.

36. Miller JM, Rochitte CE, Dewey M et al. Diagnostic Performance of Coronary Angiography by 64-Row CT. New England Jounal of Medicine 2008;359:2324-2336.

37. van Werkhoven JM, Schuijf JD, Gaemperli O et al. Prognostic value of multislice computed tomography and gated single-photon emission computed tomography in patients with suspected coronary artery disease. J Am Coll Cardiol 2009;53:623-32.

38. So A, Lee TY. Quantitative myocardial CT perfusion: a pictorial review and the current state of technology development. J Cardiovasc Comput Tomogr 2011;5:467-81.

39. Xu L, Sun Z, Fan Z. Noninvasive physiologic assessment of coronary stenoses using cardiac CT. Biomed Res Int 2015;2015:435737.

40. Danad I, Szymonifka J, Twisk JWR et al. Diagnostic performance of cardiac imaging methods to diagnose ischaemia-causing coronary artery disease when directly compared with fractional flow reserve as a reference standard: a meta-analysis. Eur Heart J 2017;38:991-998.

41. McCollough C, Leng S, Yu L, Fletcher J. Dual- and Multi-Energy CT: Principles, Technical Approaches, and Clinical Applications. Radiology 2015;276.

42. Wichmann JL, Bauer RW, Doss M et al. Dianostic Accuracy of Late Iodine-Enhancement Dual-Enegy Computed Tomography for the Detection of Chronic Myocardial Infarction Compared With Late Gadolinium-Enhancement 3-T Magnetic Resonance Imaging. Investigative Radiology 2013;48:851-856.

43. Ko SM, Choi JW, Song MG et al. Myocardial perfusion imaging using adenosine-induced stress dual-energy computed tomography of the heart: comparison with cardiac magnetic resonance imaging and conventional coronary angiography. Eur Radiol 2011;21:26-35.

44. So A, Hsieh J, Li JY, Hadway J, Kong HF, Lee TY. Quantitative myocardial perfusion measurement using CT perfusion: a validation study in a porcine model of reperfused acute myocardial infarction. Int J Cardiovasc Imaging 2012;28:1237-48.

45. Mahnken AH, Bruners P, Bornikoel CM, Kramer N, Guenther RW. Assessment of myocardial edema by computed tomography in myocardial infarction. JACC Cardiovasc Imaging 2009;2:1167-74.

46. Lee T-Y. Functional CT: physiological model. Trends in Biotechnology 2002;20:S1-S10.

47. So A, Wisenberg G, Teefy P et al. Functional CT assessment of extravascular contrast distribution volume and myocardial perfusion in acute myocardial infarction. Int J Cardiol 2018 Sep 1;266:15-23

48. Pereira R, Prato FS, Lekx KS, Sykes J, Wisenberg G. Contrast-enhanced MRI for the Assessment of Myocardial Viability After Permanent Coronary Artery Occlusion Magnetic Resonance in Medicine 2000;44:309-316.

49. Pereira R, Prato FS, Sykes J, Wisenberg G. Assessment of Myocardial Viability Using MRI During a Constant Infusion of Gd-DTPA: Further Studies at Early and Late Periods of Reperfusion. Magnetic Resonance in Medicine 1999;42:60-68.

50. Pereira R, Prato FS, Wisenberg G, Sykes J. The Determination of Myocardial Viability Using Gd-DTPA in a Canine Model of Acute Myocardial Ischemia and Reperfusion. Magnetic Resonance in Medicine 1996;36:684-693.

51. Pereira R, Prato FS, Wisenberg G, Sykes J, Yvorchuk KJ. The use of Gd-DTPA as a marker of myocardial viability in reperfused acute myocardial infarction. The International Journal of Cardiovascular Imaging 2001;17:395-404.

52. Antman EM, Anbe DT, Armstrong PW et al. ACC/AHA guidelines for the management of patients with ST-elevation myocardial infarction--executive summary: a report of the American College of Cardiology/American Heart Association Task Force on Practice Guidelines (Writing Committee to Revise the 1999 Guidelines for the Management of Patients With Acute Myocardial Infarction). Circulation 2004;110:588-636.

53. Arbab-Zadeh A, Di Carli MF, Cerci R et al. Accuracy of Computed Tomographic Angiography and Single-Photon Emission Computed Tomography-Acquired Myocardial Perfusion Imaging for the Diagnosis of Coronary Artery Disease. Circ Cardiovasc Imaging 2015;8:e003533.

54. Rochitte CE, George RT, Chen MY et al. Computed tomography angiography and perfusion to assess coronary artery stenosis causing perfusion defects by single photon emission computed tomography: the CORE320 study. Eur Heart J 2014;35:1120-30.

55. Eitel I, Desch S, Fuernau G et al. Prognostic significance and determinants of myocardial salvage assessed by cardiovascular magnetic resonance in acute reperfused myocardial infarction. J Am Coll Cardiol 2010;55:2470-9.

56. Kurita Y, Kitagawa K, Kurobe Y et al. Estimation of myocardial extracellular volume fraction with cardiac CT in subjects without clinical coronary artery disease: A feasibility study. J Cardiovasc Comput Tomogr 2016;10:237-41.

57. Kurita Y, Kitagawa K, Kurobe Y et al. Data on correlation between CT-derived and MRI-derived myocardial extracellular volume. Data Brief 2016;7:1045-1047.

58. Messroghli DR, Walters K, Plein S et al. Myocardial T1 mapping: application to patients with acute and chronic myocardial infarction. Magn Reson Med 2007;58:34-40.

59. Senthilkumar A, Majmudar M, Shenoy C, Kim HW, Kim RJ. Identifying the Etiology: A Systematic Approach Using Delayed-Enhancement Cardiovascular Magnetic Resonance. Heart Failure Clinics 2009;5:349-367.

60. Thornhill RE, Prato FS, Wisenberg G, Moran GR, Sykes J. Determining the extent to which delayed-enhancement images reflect the partition-coefficient of Gd-DTPA in canine studies of reperfused and unreperfused myocardial infarction. Magn Reson Med 2004;52:1069-79.

61. Matsuda T, Kido T, Itoh T et al. Diagnostic accuracy of late iodine enhancement on cardiac computed tomography with a denoise filter for the evaluation of myocardial infarction. Int J Cardiovasc Imaging 2015;31 Suppl 2:177-85.

62. Tanabe Y, Kido T, Kurata A et al. Late iodine enhancement computed tomography with image subtraction for assessment of myocardial infarction. Eur Radiol 2018;28:1285-1292.

63. Truong QA, Thai WE, Wai B et al. Myocardial scar imaging by standard single-energy and dual-energy late enhancement CT: Comparison with pathology and electroanatomic map in an experimental chronic infarct porcine model. J Cardiovasc Comput Tomogr 2015;9:313-20.

64. McAlindon E, Pufulete M, Lawton C, Angelini GD, Bucciarelli-Ducci C. Quantification of infarct size and myocardium at risk: evaluation of different techniques and its implications. Eur Heart J Cardiovasc Imaging 2015;16:738-46.

65. Cerqueira MD, Weissman NJ, Dilsizian V et al. Standardized Myocardial Segmentation and Nomenclature for Tomographic Imaging of the Heart. Circulation 2002;15:463-467.

66. Aletras AH, Kellman P, Derbyshire JA, Arai AE. ACUT2E TSE-SSFP: a hybrid method for T2-weighted imaging of edema in the heart. Magn Reson Med 2008;59:229-35.

67. Fuernau G, Eitel I, Franke V et al. Myocardium at risk in ST-segment elevation myocardial infarction comparison of T2-weighted edema imaging with the MR-assessed endocardial surface area and validation against angiographic scoring. JACC Cardiovasc Imaging 2011;4:967-76.

68. Ugander M, Bagi PS, Oki AJ et al. Myocardial edema as detected by pre-contrast T1 and T2 CMR delineates area at risk associated with acute myocardial infarction. JACC Cardiovasc Imaging 2012;5:596-603.

69. Kitagawa K, Sakuma H, Nagata M et al. Diagnostic accuracy of stress myocardial perfusion MRI and late gadolinium-enhanced MRI for detecting flow-limiting coronary artery disease: a multicenter study. Eur Radiol 2008;18:2808-16.

70. Bekkers SC, Yazdani SK, Virmani R, Waltenberger J. Microvascular obstruction: underlying pathophysiology and clinical diagnosis. J Am Coll Cardiol 2010;55:1649-60.

71. Dauber I, VanBenthuysen K, McMurtry I et al. Functional Coronary Microvascular Injury Evident As Increased Permeability Due to Brief Ischemia and Reperfusion. Circulation 1990;66:986-998.

72. Watabe H, Sato A, Nishina H et al. Enhancement patterns detected by multidetector computed tomography are associated with microvascular obstruction and left ventricular remodelling in patients with acute myocardial infarction. Eur Heart J 2016;37:684-92.

73. Bandula S, White S, Flett AS et al. Measurement of Myocardial Extracellular Volume Fraction by Using Equilibrium Contrast-enhanced CT: Validation against Histologic Findings. Radiology 2013;269.

74. Richardson WJ, Clarke SA, Quinn TA, Holmes JW. Physiological Implications of Myocardial Scar Structure. Compr Physiol 2015;5:1877-909.

CHAPTER 2

2 Functional CT Imaging to Identify Salvageable Myocardium for Acute Myocardial Infarction Management

2.1 Introduction

Treatment for acute myocardial infarction (AMI) aims to restore flow to stenosed arteries by percutaneous coronary intervention (PCI). PCI is effective when the procedure is performed within the first 120 minutes from symptom onset but is most successful within the first 60 minutes (1). Beyond this time window, the amount of myocardial tissue that experiences irreversible damage significantly increases (2-5). Thus, rapid recognition of AMI is required to facilitate the prompt application of PCI and to maximize its success.

Clinical symptoms and the incorporation of 12-lead electrocardiogram (ECG) are the primary basis for revascularization treatment decision-making (6). These initial assessments are sufficient to diagnose patients with ST-elevation myocardial infarction. However, for patients with non-ST elevation myocardial infarction and unstable angina, diagnosis cannot solely be made from knowledge of clinical symptoms and ECG-tracings. These patients with partial occlusions have varying degrees of AMI but are often overlooked due to the lack of significance in their preliminary tests; missing the critical window for treatment.

Many studies have explored the use of imaging to improve diagnosis and prognosis of AMI. Coronary computed tomography (CT) angiography can be useful in detecting the location and size of an occlusion (7-11). However, it yields no functional information on the hemodynamics or viability of the myocardium affected by the stenosis. The amount of salvageable myocardium estimated using functional imaging techniques is a useful metric for triaging patients; the more salvageable tissue, the more successful a revascularization treatment (12). Delayed contrast-enhanced imaging using CT and magnetic resonance imaging have shown promise in assessing myocardial viability by quantifying the retention of contrast agent at equilibrium following slow infusion (13-22).

However, this model-independent technique is impractical because of the time required to achieve equilibrium between the tissue and the arterial blood pool (typically an hour).

An indicator of myocardial viability is the presence of salvageable myocardium, or myocardium that is edematous with reduced perfusion relative to normal myocardial tissue (23-28). In contrast, non-salvageable, infarcted myocardium is edematous but has marginal to no perfusion. Salvageable myocardium is likely to become infarcted if not addressed quickly.

Recently, So *et al.* explored dynamic contrast enhanced (DCE) CT imaging to assess myocardial viability by simultaneously quantifying myocardial perfusion (MP) and edema (29). So *et al.* assumed that the extravascular contrast distribution volume (ECDV) within the injured myocardium could be a surrogate marker of edema. This metric is derived from the extended Johnson-Wilson-Lee (JWL) tracer kinetic model, but has not yet been validated by comparison to a model-independent technique. The present study aims to: (1) validate myocardial edema as measured by ECDV against the model-independent constant infusion CT imaging method, (2) derive thresholds of MP and ECDV that can be used to quantify the amount salvageable myocardium, and (3) compare the use of thresholds against the standard constant infusion CT technique to identify salvageable myocardium.

2.2 Methods

2.2.1 Study design

For this study, a porcine AMI model that exhibits injury ranging from edema to infarct was used. Although this model does not fully mimic clinical AMI, the range of injury is sufficient to evaluate different methods of myocardial tissue injury characterization. During the acute stage (3 days after AMI induction), the animals were imaged using both CT and MR. Pre-contrast and post-contrast infusion CT images were acquired to produce delayed contrast images of the heart. This constant contrast infusion technique provided a model-independent way of assessing myocardial viability as well as a standard for validating model-dependent metrics. T2-weighted turbo inversion recovery magnitude (TIRM) images were also acquired as a standard for validation. Dynamic contrast

enhanced CT images were acquired to obtain the model-dependent MP and ECDV metrics. T1 maps were acquired to derive the MP and ECDV thresholds. Imaging was repeated during the sub-acute stage (two weeks post-AMI induction). This study protocol was approved by the Western's research ethics board.

2.2.2 Animal model

Seven female Landrace pigs (40-70 kg) were used in this study. AMI was induced using a catheter-based approach, where a balloon catheter was advanced to the distal left anterior descending artery (LAD) and inflated to obstruct the downstream perfusion for one hour; perfusion was restored after one hour. Anesthesia was induced by propofol (15-20 cc, Novapharm Ltd, Scarborough, Ontario, Canada) and maintained with 2.0% isoflurane (Baxter Corporation, Mississauga, Ontario, Canada). When required, Fentanyl (Sandoz Canada Inc., Boucherville, Quebec, Canada) was administered at a dose of 1-2 mL for pain relief.

In preparation for imaging, the pig was anesthetized with 1ml/20kg Telazol (reconstituted with 5ml xylazine) IM. At 1.5 hours after initial administration of anesthetics, half the original dose was delivered to maintain heart rate. The ventilator was set at approximately 10 ml/kg (at a range of 7-15 ml/kg) to maintain low normal CO_2 range, and respiratory rate at approximately 20 bpm. Heart rate, body temperature, and partial pressure of carbon dioxide were monitored and maintained throughout the course of the scan. Ventilation was suspended approximately 2 seconds prior to the image acquisition, as needed, to mimic breatholding.

2.2.3 Data Acquisition

2.2.3.1 Computed tomography imaging

To assess injured tissue when edema is present at the acute and sub-acute stages, subjects were imaged on day 3 and day 12±3 post-AMI using CT. DCE-CT heart images were acquired with a 64-row CT750 HD scanner (GE Healthcare, Waukesha, Wisconsin) following a single bolus injection of iodine contrast agent (0.7 $mL \cdot kg^{-1}$ at 3 $mL \cdot s^{-1}$, 76% iopadimol, Isovue multipack-370). Scans were prospectively ECG gated and acquired in

the axial orientation, with a gantry speed of 0.35 s/rotation. A 3-phase protocol was used for image acquisition: 1st phase, 22 scans every 1-2 heart beats; 2nd phase, 6 scans acquired at approximately 14 s intervals; and 3rd phase, 4 scans acquired every 30 s. A dual energy technique (140/80 kVp; 0.2 ms and 630 mA) was used using a rapid switching x-ray tube.

Next, reference CT images were acquired for the constant contrast infusion protocol. Five reference images were acquired prior to the infusion of the same dose of contrast agent (0.7 $mL \cdot kg^{-1}$, 76% iopadimol, Isovue multipack-370), which was infused intravenously over one hour. Another five images were acquired post contrast infusion when the concentration of contrast in the tissue and the arterial blood pool reached equilibrium. Equilibrium was confirmed by the state of no change in enhancement between the two compartments over time. For each acquisition, 16 2.5-mm thick slices were reconstructed.

2.2.3.2 Magnetic resonance imaging

2.2.3.2.1 T2-weighted imaging for edema

T2-w images of the heart were acquired on the same day as the CT study using a 3-Tesla Siemens Magnetom Biograph mMR scanner (Siemens Healthcare, Erlangen, Germany). Similar to the CT study, each scan was acquired during the diastolic phase of the cardiac cycle following prospective ECG-gating. Ventilation was suspended for every slice location at approximately two seconds prior to scanning to mimic breatholding. The turbo inversion recovery magnitude sequence (TIRM), was used with the following scan parameters: 5 slices in the axial orientation; TE: 47ms; TR:1363ms; TI: 180ms; flip angle: 180°; ETL: 12; matrix size: 256 x 256; slice thickness: 8mm.

2.2.3.2.2 Gd enhanced T1-mapping for salvageable myocardium

In addition, a gadopentetate dimeglumine contrast (Magnevist 0.1ml/kg) enhanced T1 map was obtained with a modified Look-Locker sequence. Contrast agent was administered approximately 12 minutes prior to scanning and the scans were prospectively ECG-gated. The sequence parameters were: 202 ms acquisition window;

300ms trigger delay; three inversions at intervals of 80 ms; TR: 237.03ms; TE: 1.07ms; flip angle: 35°; ETL: 1; matrix size: 192 x 192. The same 5 8-mm thick axial slices were imaged with both sequences. Ventilation was suspended for every slice location at approximately two seconds prior to the image acquisition to mimic breatholding.

2.2.4 Data Analysis

2.2.4.1 Dynamic contrast enhanced CT

The CT projection data were reconstructed as 70 keV virtual monochromatic images (2.5 mm thick) to reduce beam-hardening artifact. To reduce the effect of cardiac and respiratory motion, partial scan reconstruction (180 degrees plus the fan angle) was utilized. (A comparison of 360-degree reconstruction and partial reconstruction is provided in Appendix A). Reconstructed images were averaged to yield seven, 5-mm thick slices covering each subject's heart. To remove the effects of residual cardiac and respiratory motion between scans, 3D images were registered using a 3D non-rigid registration algorithm (GE proprietary software) used on a GE advantage workstation (version 5.0.9).

2.2.4.1.1 ECDV and MP functional maps

For each slice, ECDV and MP functional maps were generated from a set of 70 keV virtual monochromatic DCE images using the extended JWL model of tracer kinetics, which was incorporated into the CT perfusion software (GE Healthcare). To extract an arterial input function $C_a(t)$, a region of interest was manually drawn on the descending aorta of the axial images. Myocardial regions of interest were also drawn as described in section 2.2.4.3. The mathematical descriptions used to calculate ECDV and MP were published previously by So *et al* (29). Briefly, the upslope of the tissue curve in relation to the arterial curve of the descending aorta is used to estimate the absolute MP in ml/min/g of tissue; the area under the third phase (wash-out of contrast) of the curves are used to estimate the absolute ECDV in ml/g of tissue. Figure 2-1 shows a representative DCE-CT image, along with time-enhancement curves and resulting ECDV and MP functional maps.

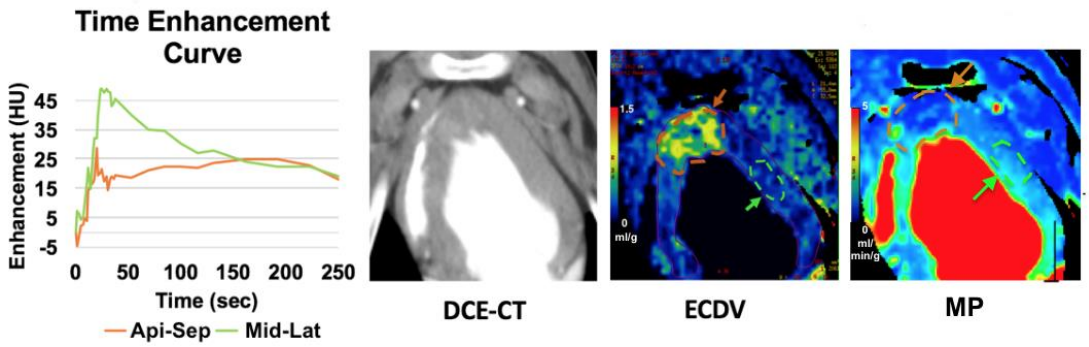

Figure 2-1 ECDV map and MP map of the left ventricular myocardium of a sub-acute phase infarcted pig post ischemic insults corresponding to the dynamic CT image. A time enhancement curve (left) of the different myocardium region outlined on the ECDV and MP map. The time enhancement curve of the injured tissue (orange) shows higher elevation than the remote during the delayed phase of the scan (50-250s), due to the retention of contrast agent.

2.2.4.2 Constant infusion CT

The constant infusion CT images were acquired and used as the reference standard because it is a model-independent approach. The measured partition coefficient value is not derived from a mathematical model but are calculated at equilibrium between the tissue and the arterial blood pool. To improve the signal-to-noise ratio (SNR), adjacent slices of the constant infusion CT acquisition were averaged into 5 mm images. Next, images acquired pre and post contrast infusion were registered to each other using the proprietary 3D non-linear registration method provided by GE, and the five pre- and five post-infusion images were averaged to further increase the signal-to-noise ratio. A difference image for each slice location was generated by subtracting the average pre-contrast image from the average post-contrast image, as shown in Figure 2-2; these difference images were then used to calculate the partition coefficient (PC) of the tissue at equilibrium. The change in signal intensity (ΔSI) between the pre and post contrast images, SI_{pre} and SI_{post} respectively, provides information on the accumulation of iodine contrast in different regions of the myocardium. Hence, PC is a surrogate marker of iodine distribution volume. The partition coefficient is calculated as the volume distribution of contrast in the total tissue region of interest (ΔSI_{tissue}) normalized to the

arterial blood pool ($\Delta SI_{arterial\ blood}$); *i.e.* PC = ΔSI_{tissue} / $\Delta SI_{arterial\ blood}$ at equilibrium. An increase in PC in infarcted myocardium corresponds to an increased contrast distribution volume as a result of edema and the additional space in which contrast can accumulate.

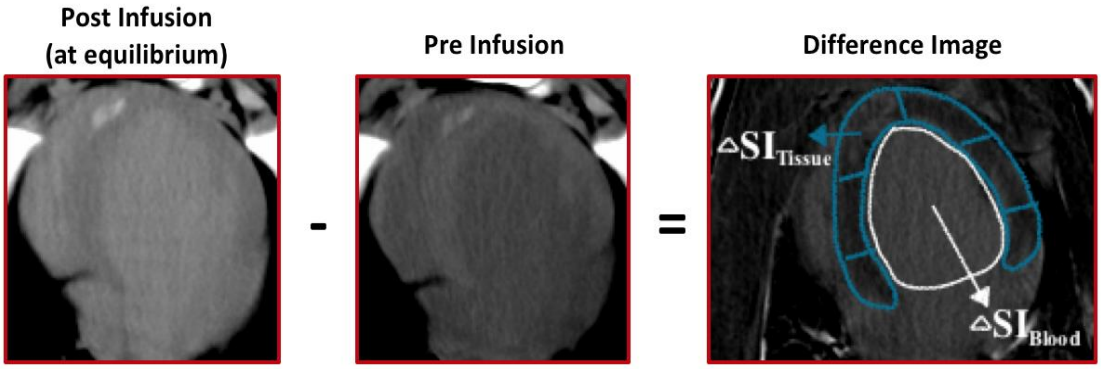

Figure 2-2 Difference image (right) generated by subtracting the pre-infusion image (center) from the post-infusion image (left).

2.2.4.3 Assignment of coronary territory

In the pig, the axial scan orientation results in myocardial images parallel to the horizontal long axis of the left ventricle (LV). Non-linearly registered DCE-CT images were averaged across time to produce a static image that was used to outline the inner and outer boundaries of the myocardium. These boundaries were used to define the myocardium on the functional maps as well as the CI difference image. The LV was divided into six segments based on the American Heart Association (AHA) horizontal long axis nomenclature (Figure 2-3) (30). The apical septal and apical lateral walls, shown in Figure 2-3 in purple and blue, respectively, are the regions supplied by the occluded LAD. Thus, these regions contain the injured tissue. The injured tissue, or the myocardium at-risk (MAR), is composed of both salvageable and infarcted myocardium. The mid-lateral wall, shown in yellow in Figure 2-3, is supplied by the patent LCx, and thus contains normal, uninjured tissue. The apical septal and the mid-lateral walls were used as regions of interest for validation of the functional CT technique at the acute and sub-acute phases after insult. The whole apical wall (septal + lateral walls) was used as a region of interest (ROI) to define the MP and ECDV thresholds.

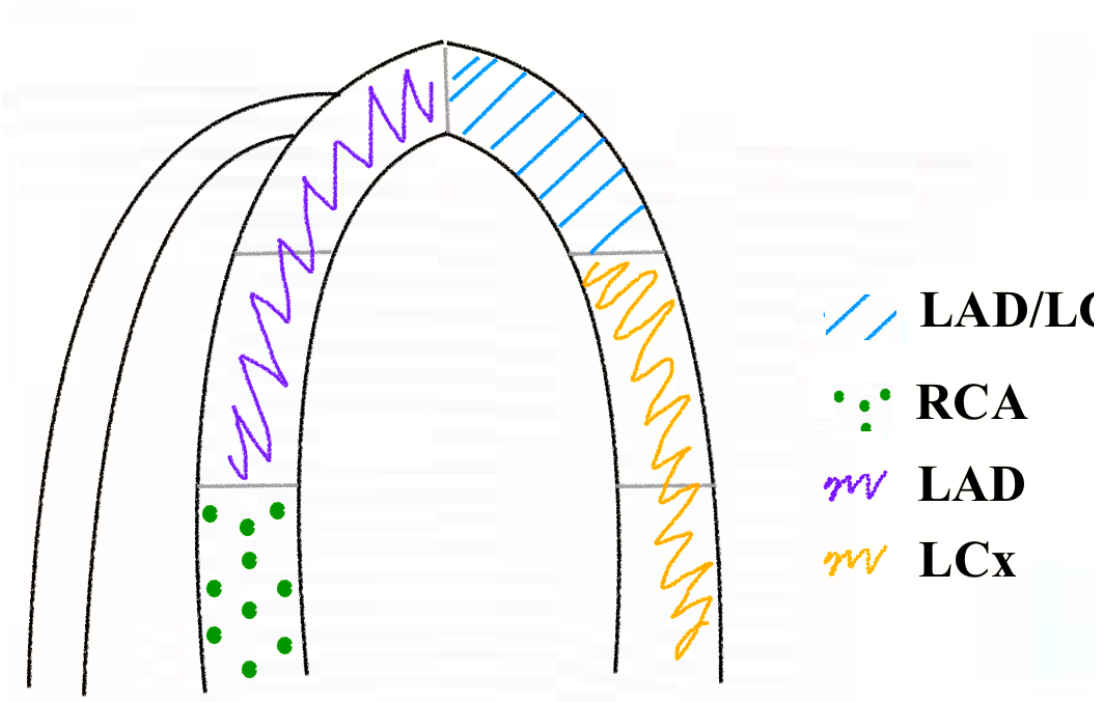

Figure 2-3 Six segment horizontal long axis of the heart as defined by the AHA (30). These segments are supplied by the left anterior descending (LAD), right coronary (RCA), and the left circumflex (LCx) arteries.

2.2.4.4 Determination of MP and ECDV thresholds that define the myocardium at-risk area

The MAR area was identified on T1 maps by selecting all pixels within the apical wall ROI with T1-values three standard deviations away from the average T1-value in the mid-lateral wall ROI. To find the corresponding MAR area within the CI difference images used to validate model-dependent metrics, a threshold of 30 HU was used, as this threshold consistently produced an MAR area that matched that measured with the T1-map. All pixels above 30 HU were considered to be MAR in pigs without microvascular obstruction (non-MVO, *n*=2).

In pigs with MVO (*n*=5), the threshold does not identify infarcted tissues, which are hypoenhanced due to lack of contrast delivery. However, these hypoenhanced regions were always surrounded by a hyperenhanced rim that is >30 HU. In these cases, the area of hyperenhanced rim was considered to be the area of salvageable myocardium, while

the hypoenhanced area was considered as the area of infarct. The sum of the areas was the MAR area.

To determine the ECDV functional map threshold that yielded an MAR area that agreed best with the MAR area determined from the CI images, the apical wall ROI in each slice was “flooded” at thresholds ranging from 0.30 ml/g to 0.50 ml/g. For each threshold, the combined area of all pixels above the threshold was calculated and compared to the MAR area determined from the CI difference images.

A similar analysis was performed on the MP functional maps. The apical wall ROI in each slice was flooded at thresholds ranging between 0.36 ml/min/g and 0.5 0ml/min/g. This range of perfusion thresholds was selected based on previous studies showing that MP <0.50 ml/min/g delineates infarcted myocardium (45,48). For each threshold, the combined area of all pixels above the threshold was calculated and compared to the infarcted area determined from the CI difference images. Since the infarcted area can only be determined in cases with MVO, this comparison was restricted to MVO subjects only. These analyses were performed using the acute phase (3 days post-AMI) images only.

2.2.4.5 Statistical analysis

All statistical analyses were performed using GraphPad Prism 7 software. Using two tailed t-tests, ECDV, PC, and T2-TIRM signal intensity (SI) values in the apical septal wall territory were compared to the ECDV, PC, and T2-TIRM SI values in the mid-lateral wall territory, respectively. Significance was determined by $p < 0.05$. Comparisons were made with images acquired at the acute and sub-acute phases. Values were reported as means of each region and standard errors between subjects.

To identify the ECDV and MP thresholds that yielded MAR and infarct areas that best agreed with the CI-defined areas, Bland-Altman analysis was performed for each threshold. The mean bias $\pm$ standard error was plotted as a function of threshold and linear regression was performed. The ECDV and MP thresholds that yielded zero bias according to the regression were selected as the thresholds that best separate injured from

uninjured tissue. Areas with ECDV greater than the threshold were considered myocardium at risk while areas with MP lower than the threshold were considered infarcted myocardium. The mean ECDV and MP values in MAR, infarcted myocardium, and normal myocardium were compared using two-tailed t-tests.

The areas of the thresholded ECDV and MP pixels within the apical wall were compared to the MAR areas determined from the CI images. A comparison between the total area of all thresholded pixels within the apical wall made (ECDV + MP) and the CI-defined MAR area was also performed. These comparisons were made using two-tailed t-tests. Both MVO and non-MVO cases were analyzed.

2.3 Results

2.3.1.1 Validation of ECDV versus constant infusion

The detection of the edematous region using the CT-derived ECDV functional map was comparable to that achieved using the CI difference image and the T2 TIRM image (Figure 2-4). ECDV in the apical septal wall during the acute (day 3) and sub-acute (day 12±3) phases post-insult was 0.39±0.04 ml/g and 0.46±0.08ml/g, respectively. As shown in Figure 2-5, the ECDV in the mid-lateral wall was significantly lower than in the apical septal wall at both the acute (0.14±0.01ml/g) and sub-acute (0.24±0.08 ml/g) phases ($p<0.05$). Similarly, PC in the mid-lateral wall was significantly lower than that in the

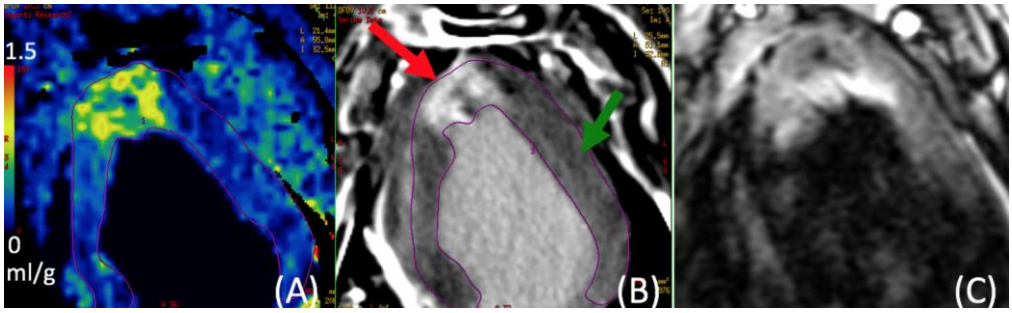

Figure 2-4 (A) ECDV MAR depicted in the apical septal wall corresponds to the enhanced region of on the CI difference image (B) and T2 TIRM image (C). Injured myocardium is shown by the enhanced region (red arrow). The normal, uninjured mid-lateral wall (green arrow) is not enhanced.

apical septal wall for both phases (acute: 0.77± 0.05 vs. 0.37±0.04 and sub-acute: 0.80±0.04 vs. 0.37±0.01, $p<0.05$).

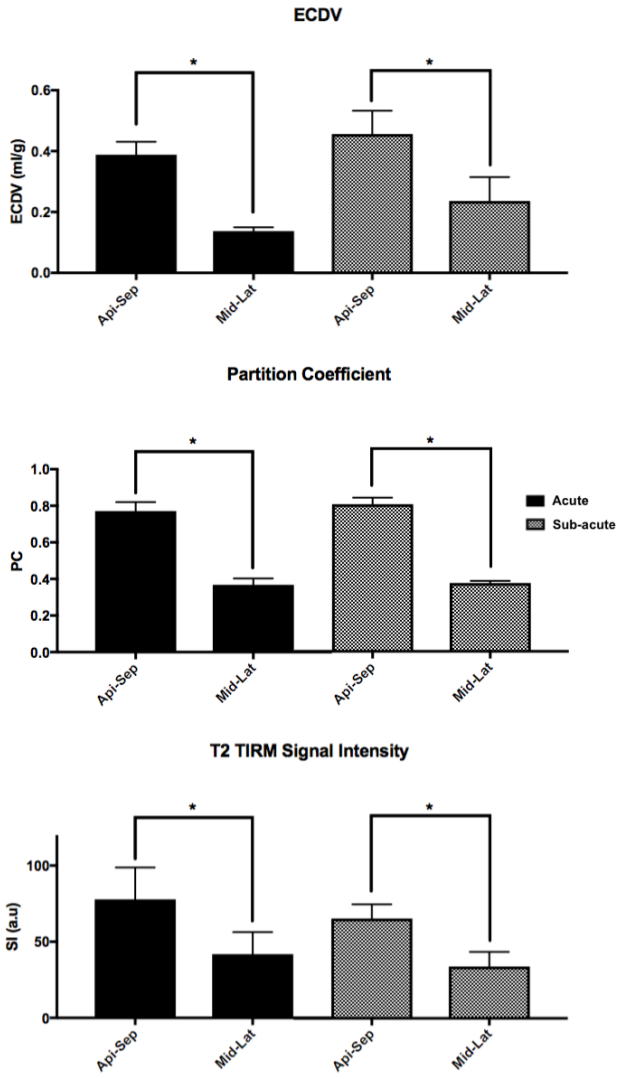

Figure 2-5 (top) ECDV (ml/g) in infarcted and normal myocardium at acute and sub-acute stages post insult. **(center)** PC in infarcted and normal myocardium at acute and sub-acute stages post insult. **(bottom)** T2 TIRM signal intensity (a.u) in infarcted and normal myocardium at acute and sub-acute stages post insult. Error bars represent standard error amongst the subjects (* denotes $p < 0.05$). Injured myocardium is represented by the apical-septal wall and the uninjured normal myocardium is represented by the mid-lateral wall**.**

Change in ECDV and PC between normal and MAR within each subject is shown in Figure 2-6. The same result was also observed in the T2-TIRM images. The signal

intensities in the mid-lateral wall were significantly lower than the signal intensities in the apical septal wall for both the acute and sub-acute phases. The corresponding signal intensities in the at-risk and normal myocardium on acute and sub-acute phase T2 TIRM images were 77.8±21.0 vs. 41.9±14.4 and 65.6±9.20 vs. 34.0±9.68 ($p<0.05$), respectively.

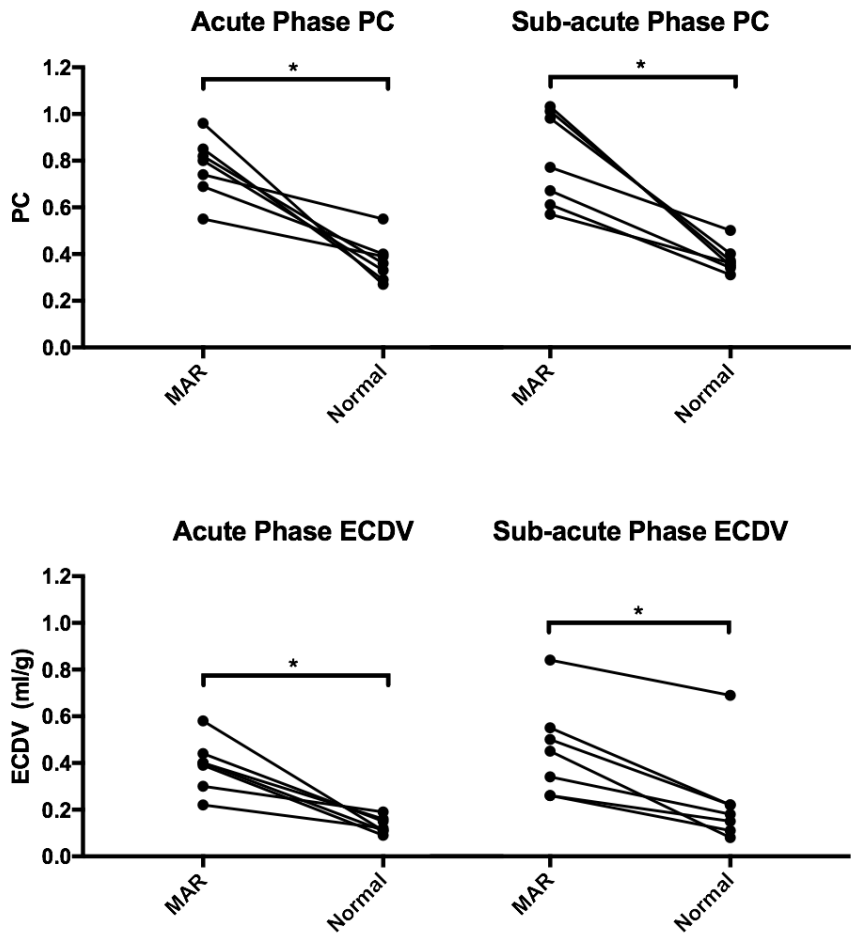

Figure 2-6 (top) Difference of partition coefficient between MAR and remote normal tissue is shown for each of the seven pigs at the acute and sub-acute phases. **(bottom)** The same trends are seen for ECDV. (* denotes $p < 0.05$).

2.3.1.2 ECDV and MP thresholds

The mean bias between the thresholded ECDV area and the CI-derived MAR area are plotted with respect to ECDV threshold value in Figure 2-7, along with the mean bias between the thresholded MP area and the CI-derived infarct area, which are plotted with

respect to MP threshold. Linear fitting determined that an ECDV threshold of 0.36 ml/g and an MP threshold of 0.44 ml/min/g resulted in a mean bias of zero. The corresponding R-squared values for the linear fits were 0.99 for both MP and ECDV.

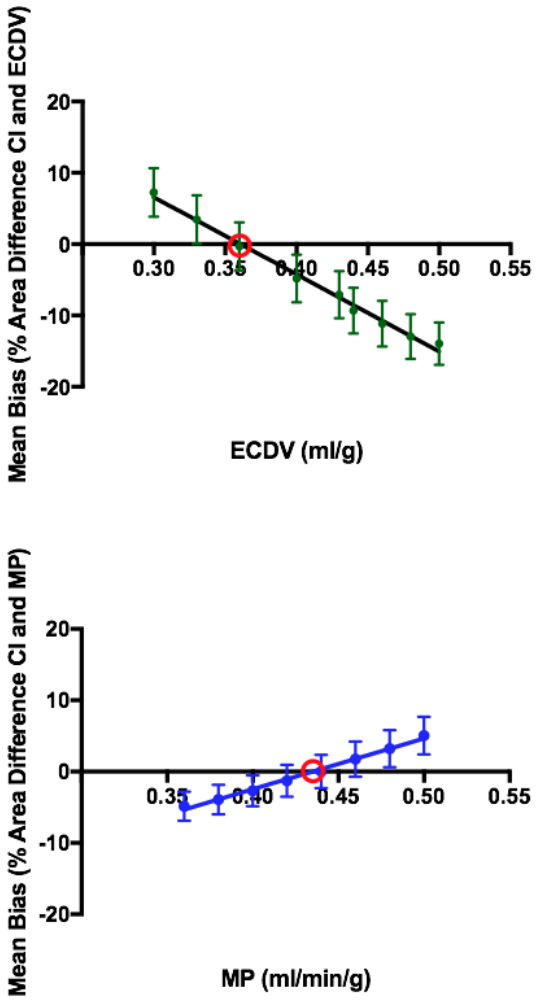

Figure 2-7 (top) Mean bias of percent area difference between CI and ECDV plotted on the y-axis. ECDV range plotted on the x-axis ECDV threshold of mean bias zero to delineate MAR is 0.36 ml/g for acute phase MVO and non-MVO cases. **(bottom)** Mean bias of percent area difference between CI and MP plotted on the y-axis. MP range plotted on the x-axis. MP threshold of mean bias zero to delineate infarct is 0.44 ml/min/g for acute phase MVO cases. Error bars represent the standard error.

The derived MP and ECDV thresholds were used to determine the mean ECDV and MP values in MAR, infarcted myocardium, and normal myocardium (Figure 2-8). As expected, mean ECDV in normal myocardium < MAR < infarcted myocardium; mean

MP in normal myocardium > MAR > infarcted myocardium. The mean MP ± standard error of infarcted myocardium, MAR, and normal myocardium were 0.30±0.07 ml/min/g, 0.81±0.19 ml/min/g, 0.93±0.27 ml/min/g, respectively. The mean ECDV ± standard error of infarcted myocardium, MAR, and normal myocardium were 0.61±0.12 ml/g, 0.22±0.07 ml/g, 0.13±0.07 ml/g, respectively. ECDV and MP can distinguish normal and

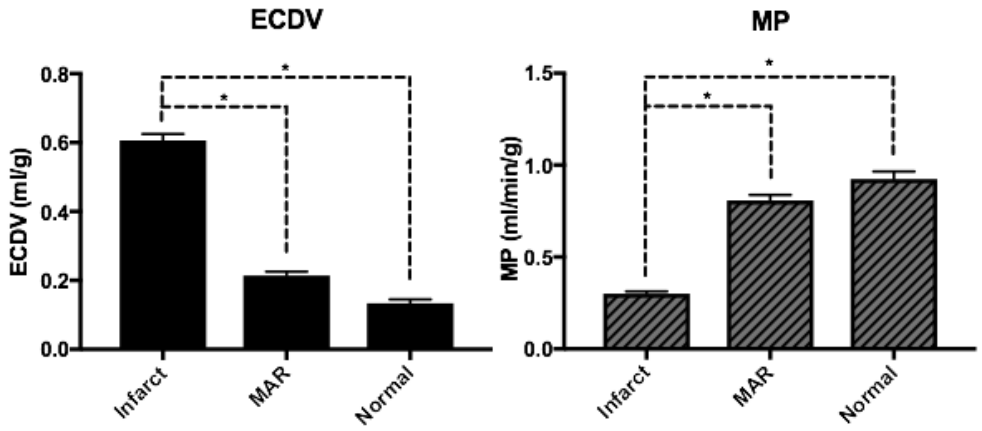

Figure 2-8 Mean MP (ml/min/g) and mean ECDV (ml/g) within different tissue states: infarct, at-risk, and normal, determined by MP and ECDV thresholds of 0.44 ml/min/g and 0.36 ml/g, respectively. Error bars represent standard error of forty-two slices from 7 pigs. (* denotes $p < 0.05$).

infarcted myocardium ($p < 0.05$). ECDV and MP values were also able to distinguish infarcted myocardium from MAR ($p<0.05$); however, no statistical difference was seen in ECDV and MP measurements between MAR and normal myocardium.

2.3.1.3 Combining ECDV and MP to assess MAR

The apical wall ROI of an ECDV functional map flooded at 0.36 ml/g can identify MAR, but cannot identify infarcted myocardium in subjects with MVO (n=5), as shown in Figure 2-9, left. However, the apical wall ROI of a MP functional map can identify infarcted myocardium at 0.44 ml/min/g. Figure 2-10 (bottom) shows the infarcted myocardium determined by the MP threshold match the unidentifiable area on the ECDV map at its derived threshold, when the maps are overlaid in subjects with MVO. In a subject with no MVO (n=2), the apical wall ROI of a ECDV functional map flooded at 0.36ml/g can identify MAR, as illustrated in Figure 2-9, right. The apical wall ROI of a

MP functional map flooded at 0.44ml/min/g can identify infarcted myocardium. The infarcted myocardium is identified as a small area within a large area of MAR (Figure 2-10, top)

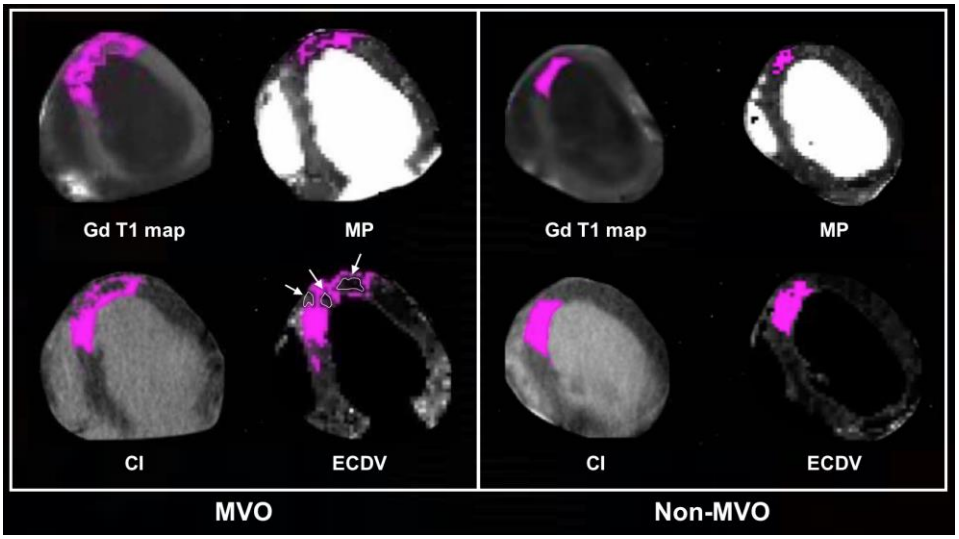

Figure 2-9 (left) contrast enhanced T1 map, CI difference image, MP, and ECDV maps of a single subject (center slice) with MVO and with minimal MVO **(right)** The colored regions correspond to the pixels flooded at specific thresholds. The ECDV scale is 0 to 1.2ml/g and MP scale from 0 to 5.0ml/min/g). The white arrows point to regions of MVO.

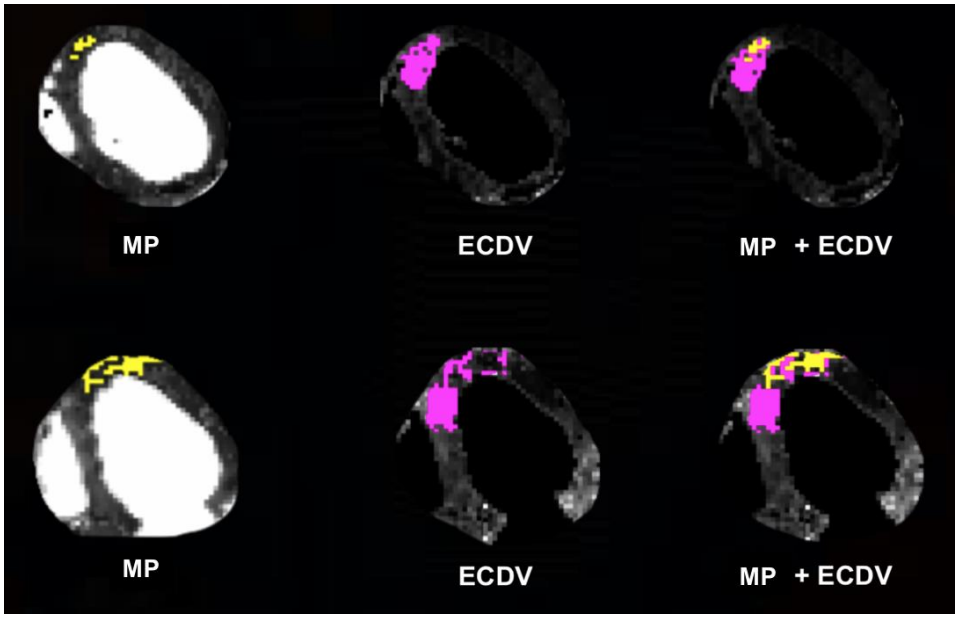

Figure 2-10 (top) subject with minimal MVO **(bottom)** subject with massive MVO. Yellow = infarcted myocardium estimated at MP <0.44ml/min/g. Pink = MAR in non-MVO cases and salvageable myocardium in MVO cases determined as ECDV >0.36ml/g. ECDV scale 0 to 1.2 ml/g and MP scale from 0 to 5.0 ml/min/g.

The areas of the thresholded ECDV and MP pixels within the apical wall was compared to the MAR area determined from the CI images, grouped into MVO and non-MVO cases. A comparison was also performed between the total area of all thresholded pixels within the apical wall (ECDV + MP) and the CI-defined MAR area in the group subjected to MVO. For the group with no MVO, a comparison was completed between the subtracted area of MP thresholded pixels from the area of ECDV thresholded pixels within the apical wall ROI (ECDV - MP) and the CI-defined MAR area. Figure 2-11 (left) demonstrates a significant difference between the area of MAR measured through CI difference imaging and MP ($p<0.0001$) or ECDV ($p<0.001$) alone. No statistical significance was seen between MAR area calculated as the total area of MP and ECDV (ECDV + MP), and the MAR area acquired through CI difference image ($p>0.05$). Figure 2-11 (right) exhibited significant difference between the area of MAR measured through CI difference imaging and MP ($p<0.005$). In addition, statistical significance was seen between MAR area calculated by subtracting MP thresholded pixels from an area of ECDV threshold pixels (ECDV-MP), and the MAR area acquired through CI difference image ($p<0.005$). No significant difference was seen MAR area estimated using ECDV alone and CI difference image ($p>0.05$).

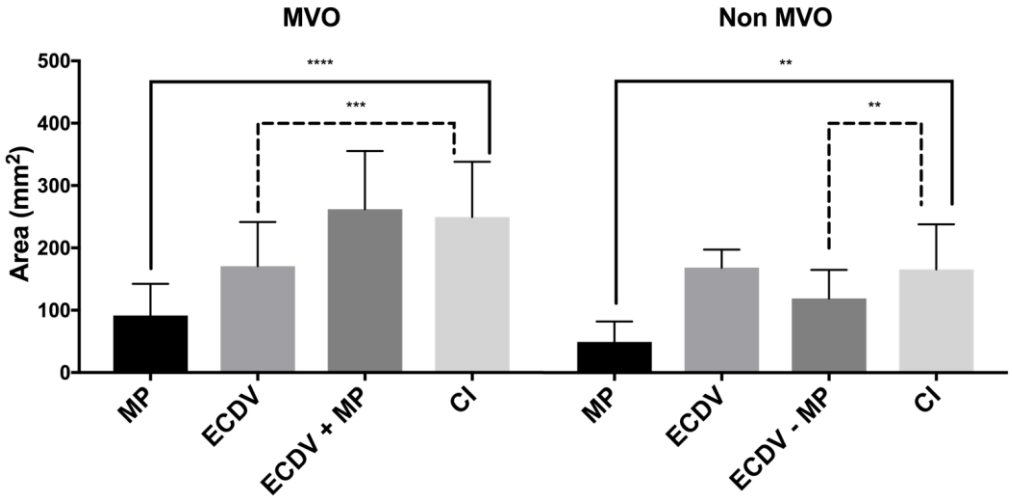

Figure 2-11 (left) MVO cases (n=5), comparing the area of infarct (MP), salvageable myocardium (ECDV), myocardium at risk (ECDV+MP) to the myocardium at risk area measured using CI. **(right)** non-MVO cases (n=2), comparing the area of infarct (MP), myocardium at risk (ECDV), salvageable myocardium (ECDV+MP) to the myocardium at risk area measured using CI. Error bars represent the standard error amongst each slice between subjects. ** $p < 0.005$, *** $p < 0.001$, **** $p < 0.0001$.

2.4 Discussion

In this study, the ECDV metric derived from the extended JWL tracer kinetic model was used as a surrogate marker of edema in AMI. Our results demonstrated that the absolute measurements of ECDV were higher in the apical-septal wall relative to the mid-lateral wall. These findings were comparable to the patterns of edema measured using the model-independent constant infusion CT method and T2 TIRM MR images; and were indicative of edema in the extravascular space allowing greater retention of contrast (24,26,27,31). Following the validation of myocardial edema as measured by ECDV against the model-independent constant infusion CT imaging method, thresholds of MP and ECDV were derived to be used to quantify the amount salvageable myocardium. This study demonstrated the potential use for functional CT in quantifying the area of salvageable myocardium, yielding comparable area of salvageable myocardium estimated using the model independent constant infusion CT technique.

MP and ECDV thresholds determined based on our analysis on subjects of MVO and non-MVO, imaged at the acute phase after infarct were 0.44 ml/min/g and 0.36 ml/g, respectively. MP less than 0.44 ml/min/g delineated the infarcted myocardium that is irreversibly damaged despite revascularization of the occluded artery. On the other hand, ECDV values greater than 0.36 ml/g were indicative of MAR or salvageable tissue. Although a strict threshold is determined, MP threshold of 0.44 ± 0.02 ml/min/g (or 3% deviance from mean bias of zero) and ECDV threshold of 0.36 ± 0.03 ml/g (or 5% deviance from mean bias of zero) is an acceptable range to identify areas of MAR and infarcted myocardium.

In injured myocardium with high degree of MVO, the area of infarcted myocardium plays a significant role and is prominent within the MAR. The salvageable myocardium estimated in MVO cases will be minimal compared to non-MVO cases as the size of infarcted myocardium in non-MVO cases with be minimal.

Previous studies have shown elevation in edema in injured myocardium using T2-w MR imaging, which this study has confirmed in the acute and sub-acute phase after AMI (23,31-34). In addition, model independent delayed enhancement CT and MR imaging

were explored in other studies to assess MAR, with the assumption that retention of contrast at equilibrium is a measure of excess space and fluid in the injured myocardium 17,18,20,22,34). The present study has tested the ECDV technique against a model independent constant infusion CT imaging technique, which also assumes the retention of contrast in injured myocardium to assess MAR.

Prolonged coronary artery occlusion in the absence of revascularization treatment leads to damage at the microvascular level caused by inflammation, as a result of reperfusion (35-37). The presence of MVO has been observed clinically and during animal-model studies. The degree of MVO yields prognostic value; hence, MVO is of interest in the imaging community during the investigation of salvageable myocardium. Contrast enhanced T1 and T2-w MR imaging has been used concomitantly to assess salvageable myocardium, and many of these studies were promising (12,33,34). Similar to our results, late gadolinium enhanced MR images and gadolinium enhanced T1 maps displayed patterns of hyperenhanced myocardium regions within a hypoenhanced myocardium rim. The opposite pattern is seen in MR from CT because gadolinium shortens the T1 relaxation time, making the myocardium with contrast accumulation appear hypoenhanced. This pattern detected with contrast enhanced MR is an imaging technique used in the clinic to asses MVO (35). Comparable assessment of MVO injury can be accomplished using MP and ECDV metrics estimated using the functional CT technique. Consequently, the functional CT technique can be used to delineate salvageable myocardium similar to MR imaging.

A limitation of this study was the variation in slice thickness between the MR and CT images. The T2 TIRM and contrast enhanced T1-map used for this study were 8 mm in slice thickness. In contrast, the CT images were reconstructed at 5 mm slice thicknesses. Although the center slices were selected for the validation across modality, slight differences in location of the heart can be detected. To address this study limitation, images acquired using the four imaging techniques (T1 mapping, T2 TIRM, CI CT, DCE CT) should be co-registered with each other to ensure the alignment of the images. Another limitation of this study that must be addressed in the future is the lack of non-

MVO subjects (n=2). To confirm our findings, a greater sample population of non-MVO cases is needed.

Another major limitation that should be addressed in future studies is the prognostic value of using ECDV and MP to triage patients for revascularization. Salvageable myocardium delineated through ECDV and MP thresholds were not compared to the ejection fraction measurements prior to revascularization. Whether or not ECDV and MP provide comparable diagnostic and prognostic value as ejection fraction measurements should be further investigated.

2.5 Conclusion

Partition coefficient, at equilibrium, has been validated (using MRI) as a means to assess myocardial viability using CT. Unfortunately, in both MRI and CT, equilibrium between tissue and the arterial blood pool can only be reached following prolonged constant infusion of contrast agent, rendering such studies impractical for clinical use. The functional CT technique proposed by So *et al*.(29), which introduced the extended JWL tracer kinetic model to measure ECDV and MP simultaneously during a single imaging session, data are acquired over only 4 minutes. The present study validated ECDV and MP measured in an animal model of AMI and identified that a threshold of 0.36 ml/g and 0.44ml/min/g can delineate area of MAR and infarct myocardium; which can then be used to estimate salvageable myocardium. The estimation of salvageable myocardium will be useful in triaging patients for revascularization treatment for particularly NSTEMI, UA, and late-arriving patients.

2.6 Reference

1. Antman EM, Anbe DT, Armstrong PW et al. ACC/AHA guidelines for the management of patients with ST-elevation myocardial infarction--executive summary: a report of the American College of Cardiology/American Heart Association Task Force on Practice Guidelines (Writing Committee to Revise the 1999 Guidelines for the Management of Patients With Acute Myocardial Infarction). Circulation 2004;110:588-636.

2. Bagai A, Dangas GD, Stone GW, Granger CB. Reperfusion strategies in acute coronary syndromes. Circ Res 2014;114:1918-28.

3. De Luca G, Suryapranata H, Ottervanger JP, Antman EM. Time delay to treatment and mortality in primary angioplasty for acute myocardial infarction: every minute of delay counts. Circulation 2004;109:1223-5.

4. Francone M, Bucciarelli-Ducci C, Carbone I et al. Impact of primary coronary angioplasty delay on myocardial salvage, infarct size, and microvascular damage in patients with ST-segment elevation myocardial infarction: insight from cardiovascular magnetic resonance. J Am Coll Cardiol 2009;54:2145-53.

5. Guerchicoff A, Brener SJ, Maehara A et al. Impact of delay to reperfusion on reperfusion success, infarct size, and clinical outcomes in patients with ST-segment elevation myocardial infarction: the INFUSE-AMI Trial (INFUSE-Anterior Myocardial Infarction). JACC Cardiovasc Interv 2014;7:733-40.

6. Amsterdam EA, Wenger NK, Brindis RG et al. 2014 AHA/ACC Guideline for the Management of Patients with Non-ST-Elevation Acute Coronary Syndromes: a report of the American College of Cardiology/American Heart Association Task Force on Practice Guidelines. J Am Coll Cardiol 2014;64:e139-e228.

7. Arbab-Zadeh A, Di Carli MF, Cerci R et al. Accuracy of Computed Tomographic Angiography and Single-Photon Emission Computed Tomography-Acquired Myocardial Perfusion Imaging for the Diagnosis of Coronary Artery Disease. Circ Cardiovasc Imaging 2015;8:e003533.

8. Danad I, Szymonifka J, Twisk JWR et al. Diagnostic performance of cardiac imaging methods to diagnose ischaemia-causing coronary artery disease when directly compared with fractional flow reserve as a reference standard: a meta-analysis. Eur Heart J 2017;38:991-998.

9. Goldstein JA, Chinnaiyan KM, Abidov A et al. The CT-STAT (Coronary Computed Tomographic Angiography for Systematic Triage of Acute Chest Pain Patients to Treatment) trial. J Am Coll Cardiol 2011;58:1414-22.

10. Miller JM, Rochitte CE, Dewey M et al. Diagnostic Performance of Coronary Angiography by 64-Row CT. New England Journal of Medicine 2008;359:2324-2336.

11. Rochitte CE, George RT, Chen MY et al. Computed tomography angiography and perfusion to assess coronary artery stenosis causing perfusion defects by single photon emission computed tomography: the CORE320 study. Eur Heart J 2014;35:1120-30.

12. Eitel I, Desch S, Fuernau G et al. Prognostic significance and determinants of myocardial salvage assessed by cardiovascular magnetic resonance in acute reperfused myocardial infarction. J Am Coll Cardiol 2010;55:2470-9.

13. Kurita Y, Kitagawa K, Kurobe Y et al. Estimation of myocardial extracellular volume fraction with cardiac CT in subjects without clinical coronary artery disease: A feasibility study. J Cardiovasc Comput Tomogr 2016;10:237-41.

14. Kurita Y, Kitagawa K, Kurobe Y et al. Data on correlation between CT-derived and MRI-derived myocardial extracellular volume. Data Brief 2016;7:1045-1047.

15. Messroghli DR, Walters K, Plein S et al. Myocardial T1 mapping: application to patients with acute and chronic myocardial infarction. Magn Reson Med 2007;58:34-40.

16. Senthilkumar A, Majmudar M, Shenoy C, Kim HW, Kim RJ. Identifying the Etiology: A Systematic Approach Using Delayed-Enhancement Cardiovascular Magnetic Resonance. Heart Failure Clinics 2009;5:349-367.

17. Thornhill RE, Prato FS, Wisenberg G, Moran GR, Sykes J. Determining the extent to which delayed-enhancement images reflect the partition-coefficient of Gd-DTPA in canine studies of reperfused and unreperfused myocardial infarction. Magn Reson Med 2004;52:1069-79.

18. Matsuda T, Kido T, Itoh T et al. Diagnostic accuracy of late iodine enhancement on cardiac computed tomography with a denoise filter for the evaluation of myocardial infarction. Int J Cardiovasc Imaging 2015;31 Suppl 2:177-85.

19. Pereira R, Prato FS, Sykes J, Wisenberg G. Assessment of Myocardial Viability Using MRI During a Constant Infusion of Gd-DTPA: Further Studies at Early and Late Periods of Reperfusion. Magnetic Resonance in Medicine 1999;42:60-68.

20. Tanabe Y, Kido T, Kurata A et al. Late iodine enhancement computed tomography with image subtraction for assessment of myocardial infarction. Eur Radiol 2018;28:1285-1292.

21. Truong QA, Thai WE, Wai B et al. Myocardial scar imaging by standard single-energy and dual-energy late enhancement CT: Comparison with pathology and

electroanatomic map in an experimental chronic infarct porcine model. J Cardiovasc Comput Tomogr 2015;9:313-20.

22. Wichmann JL, Bauer RW, Doss M et al. Dianostic Accuracy of Late Iodine-Enhancement Dual-Enegy Computed Tomography for the Detection of Chronic Myocardial Infarction Compared With Late Gadolinium-Enhancement 3-T Magnetic Resonance Imaging. Investigative Radiology 2013;48:851-856.

23. Abdel-Aty H, Cocker M, Meek C, Tyberg JV, Friedrich MG. Edema as a very early marker for acute myocardial ischemia: a cardiovascular magnetic resonance study. J Am Coll Cardiol 2009;53:1194-201.

24. Friedrich MG. Myocardial edema--a new clinical entity? Nat Rev Cardiol 2010;7:292-6.

25. Friedrich MG, Kim HW, Kim RJ. T2-weighted imaging to assess post-infarct myocardium at risk. JACC Cardiovasc Imaging 2011;4:1014-21.

26. Garcia-Dorado D, Andres-Villarreal M, Ruiz-Meana M, Inserte J, Barba I. Myocardial edema: a translational view. J Mol Cell Cardiol 2012;52:931-9.

27. Mahnken AH, Bruners P, Bornikoel CM, Kramer N, Guenther RW. Assessment of myocardial edema by computed tomography in myocardial infarction. JACC Cardiovasc Imaging 2009;2:1167-74.

28. McAlindon E, Pufulete M, Lawton C, Angelini GD, Bucciarelli-Ducci C. Quantification of infarct size and myocardium at risk: evaluation of different techniques and its implications. Eur Heart J Cardiovasc Imaging 2015;16:738-46.

29. So A, Wisenberg G, Teefy P et al. Functional CT assessment of extravascular contrast distribution volume and myocardial perfusion in acute myocardial infarction. Int J Cardiol 2018 Sep 1; 266:15-23

30. Cerqueira MD, Weissman NJ, Dilsizian V et al. Standardized Myocardial Segmentation and Nomenclature for Tomographic Imaging of the Heart. Circulation 2002;15:463-467.

31. Walls MC, Verhaert D, Min JK, Raman SV. Myocardial edema imaging in acute coronary syndromes. J Magn Reson Imaging 2011;34:1243-50.

32. Aletras AH, Kellman P, Derbyshire JA, Arai AE. ACUT2E TSE-SSFP: a hybrid method for T2-weighted imaging of edema in the heart. Magn Reson Med 2008;59:229-35.

33. Fuernau G, Eitel I, Franke V et al. Myocardium at risk in ST-segment elevation myocardial infarction comparison of T2-weighted edema imaging with the MR-assessed endocardial surface area and validation against angiographic scoring. JACC Cardiovasc Imaging 2011;4:967-76.

34. Ugander M, Bagi PS, Oki AJ et al. Myocardial edema as detected by pre-contrast T1 and T2 CMR delineates area at risk associated with acute myocardial infarction. JACC Cardiovasc Imaging 2012;5:596-603.

35. Bekkers SC, Yazdani SK, Virmani R, Waltenberger J. Microvascular obstruction: underlying pathophysiology and clinical diagnosis. J Am Coll Cardiol 2010;55:1649-60.

36. Dauber I, VanBenthuysen K, McMurtry I et al. Functional Coronary Microvascular Injury Evident As Increased Permeability Due to Brief Ischemia and Reperfusion. Circulation 1990;66:986-998.

37. Watabe H, Sato A, Nishina H et al. Enhancement patterns detected by multidetector computed tomography are associated with microvascular obstruction and left ventricular remodelling in patients with acute myocardial infarction. Eur Heart J 2016;37:684-92.

CHAPTER 3

3 Conclusions and Future Work

The purpose of this chapter is to summarize the achievements of my thesis, provide general conclusions, address the limitations of the research and provide suggestions for the future work that can ultimately lead to the clinical use of DCE-CT in estimating salvageable myocardial tissue.

3.1 Summary of Thesis Work

AMI is a leading cause of morbidity and mortality in America. A functional imaging technique is needed to assess salvageable myocardium for proper patient management for revascularization treatment. This will be useful to ensure that the patients who would most likely benefit from treatment after MI are guaranteed revascularization treatment within the window of opportunity. My thesis investigated the use of functional CT data generated from a series of DCE images to which a tracer kinetic model that best represented the pathophysiology of AMI was applied to delineate area of salvageable myocardium.

Prior to my contributions to this area of research, Dr. Aaron So and Dr. Ting-Yim Lee pioneered the extended JWL model of tracer kinetics to model the exchange of contrast between different compartments of an injured myocardium (1-4). They defined this distribution of contrast using ECDV and MP, and these parameters were validated against the native T1-map and T2-w MR as reference in a previous paper (2). I began my contribution to this thesis work by confirming Dr. So's previous validation study with T2-TIRM MR imaging and in addition, compared the ECDV measurements to a model-independent constant infusion CT-based measurement. ECDV estimated from the functional CT technique demonstrated an elevation in edema in injured myocardium relative to normal myocardium. These findings validated that ECDV is a surrogate measure of myocardial edema.

After validating ECDV as a surrogate measure of edema, against the previously established standard of constant infusion, I investigated the potential clinical utility of the

functional CT technique. Prior literature has demonstrated the usefulness of myocardial perfusion imaging in detecting injured myocardium following ischemic injury (2-11). MP together with the recent advent of ECDV can be used to characterize different components of ischemically injured myocardium, which can be used to assess salvageable myocardium. Therefore, I evaluated the hypothesis that the combination of simultaneously acquired MP and ECDV functional maps would enable the detection of infarcted myocardium, MAR, and salvageable myocardium. Firstly, as demonstrated in Chapter 2, MP and ECDV thresholds, determined at the acute phase post insult, indicate that MP lower than 0.44 ml/min/g represents infarcted myocardium, and ECDV values greater than 0.36 ml/g represent MAR area. I concluded that the combination of these two quantitative metrics was useful in determining the area of salvageable myocardium. Section 3.3.4 will further discuss the importance of estimating both salvageable myocardium and MAR for careful triage of patients for revascularization treatment.

3.2 Study Limitations

There are several limitations to the study presented in Chapter 2. First, this study was limited to seven subjects, which may not suffice given that only two of these subjects were non-MVO. The number of animals with non-MVO were underrepresented in this study, and more animals are required to represent the patient population in clinical settings. Secondly, the porcine animal model was not the ideal model of AMI. The animal AMI model consisted of ischemia followed by reperfusion. This can mimic the process of MI in UA and NSTEMI patients, but does not represent STEMI patients with complete occlusions that do not reperfuse.

Although the validation of the functional CT technique was completed on acute and sub-acute phases after MI, evaluation of ECDV and MP to assess salvageable myocardium was performed during acute phase after MI. Evaluation of ECDV and MP to estimate salvageable myocardium in sub-acute and chronic MI in a greater population of animals will be valuable.

Another technical limitation of this study was the variation in slice thickness between the MR and CT images. The T2-w and gadolinium T1-map used for this study were 8 mm

thick and the CT images were reconstructed at 5 mm slice thickness. Although the center slices were used for analysis, slight differences in location of the heart can be detected.

The above limitation leads us to our second major limitation of this thesis work, which is the absence of co-registration between different imaging methods. For example, slight variation in slice location was seen between MR and CT, as well as between DCE-CT and CI-CT. The later variation is due to the change in the subject's heart rate between the two acquired scans. This could have been minimized by co-registration of the images, but due to the lack of rigidity in cardiac images and cardiac residual motion, attempts to do so was unsuccessful.

3.3 Future Work

3.3.1 Monochromatic energy level to improve ECDV estimation

An advantage of dual energy CT used to image the subjects of this study is its ability to use two different x-ray energies from a single energy source, to retrospectively reconstruct a virtual monochromatic image. As implemented on the GE scanner, virtual monochromatic images can be reconstructed at different energy levels. To reduce beam-hardening artefacts, our previous studies (including the work in my thesis) used virtual monochromatic images reconstructed at 70 keV. However, because the k-edge of iodine is at 33 keV, we hypothesise that reconstructing virtual monochromatic images at an energy closer to the k edge would result in higher contrast to noise ratio (CNR) of iodine enhancement in the injured myocardium relative to the normal tissue, ECDV at two different monochromatic energy levels were investigated.

In a preliminary evaluation, I reconstructed virtual monochromatic images at 50 keV for six subjects (acute phase post insult), in addition to the 70 keV maps of Chapter 2, and generated ECDV maps at 50 and 70 keV. Representative ECDV maps generated at 50 and 70 keV are shown in Figure 3-1. No significant difference was observed in normal and injured myocardium between ECDV measurements estimated using retrospectively reconstructed 50 keV and 70 keV monochromatic DCE-CT (Figure 3-2).

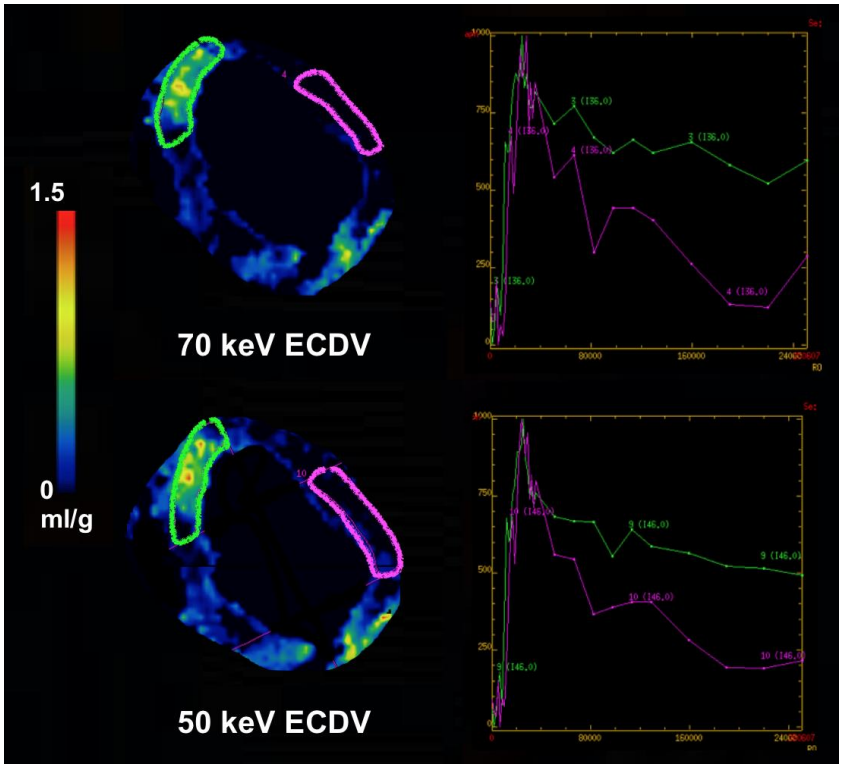

Figure 3-1 ECDV functional maps generated at 70 keV and 50 keV of a single subject. Graphs on the right illustrate the normalized time enhancement curves of the injured apical septal wall (green) and normal mid-lateral myocardium (purple).

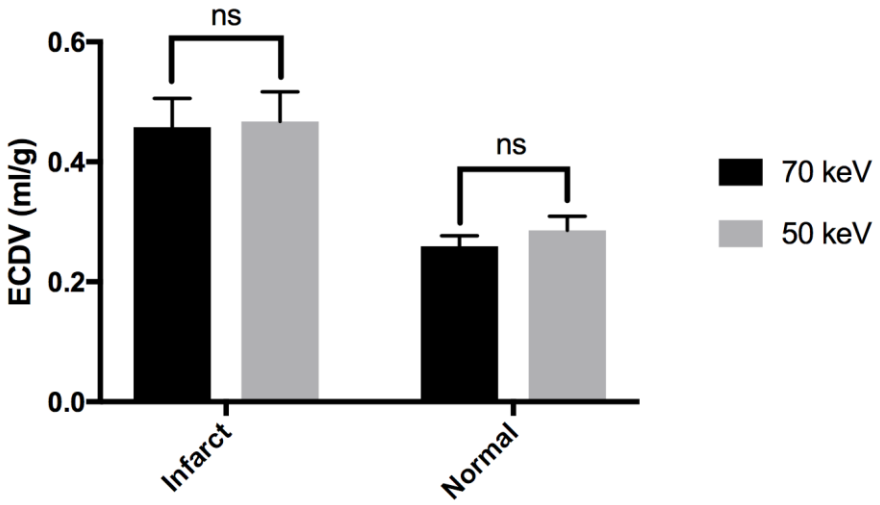

Figure 3-2 ECDV measurements (n=6) compared between images produced using 70 keV and 50 keV partial scan data. Error bars represent the standard error of the mean. (ns denotes no significance ($p > 0.05$)).

While our preliminary results yielded no statistical significance, further investigation must be performed to understand why CNR did not improve in ECDV functional maps generated from a monochromatic image closer to the k-edge of iodine.

3.3.2 Validation of four-minute scan duration in estimating ECDV

The functional CT technique for estimating ECDV is performed in approximately four minutes. It consists of three phases: 1st phase: 22 axial scans at every 1-2 s, 2nd phase: 6 axial scans at every 14 s, 3rd phase: 4 axial scans at every 30 s. However, other labs have emphasized that prolonged scan times - of up to ten minutes – are required to allow for the measurement of the greatest amount of contrast retention in the injured myocardium (12,13). To validate that our short, four-minute, dynamic imaging session is sufficient for accurate estimation of ECDV, future work should compare ECDV measured from scans that include a fourth phase that lasts up to 10 min. To provide preliminary validation, I analysed data from two subjects, with acute AMI, which were scanned for up to ten minutes; the additional 4th phase consisted of 6 axial scans acquired at 60 s intervals. ECDV functional maps were generated using all four phases and compare to the ECDV functional maps processed using only the three-phase data. The ECDV measurements were compared in infarcted and normal myocardium. Figure 3-3 suggests that the additional scans acquired up to 10 minutes do not change the measured ECDV. However, further study is required to provide statistical significance and to evaluate equivalence in cases with minimal perfusion, such as high degree of MVO.

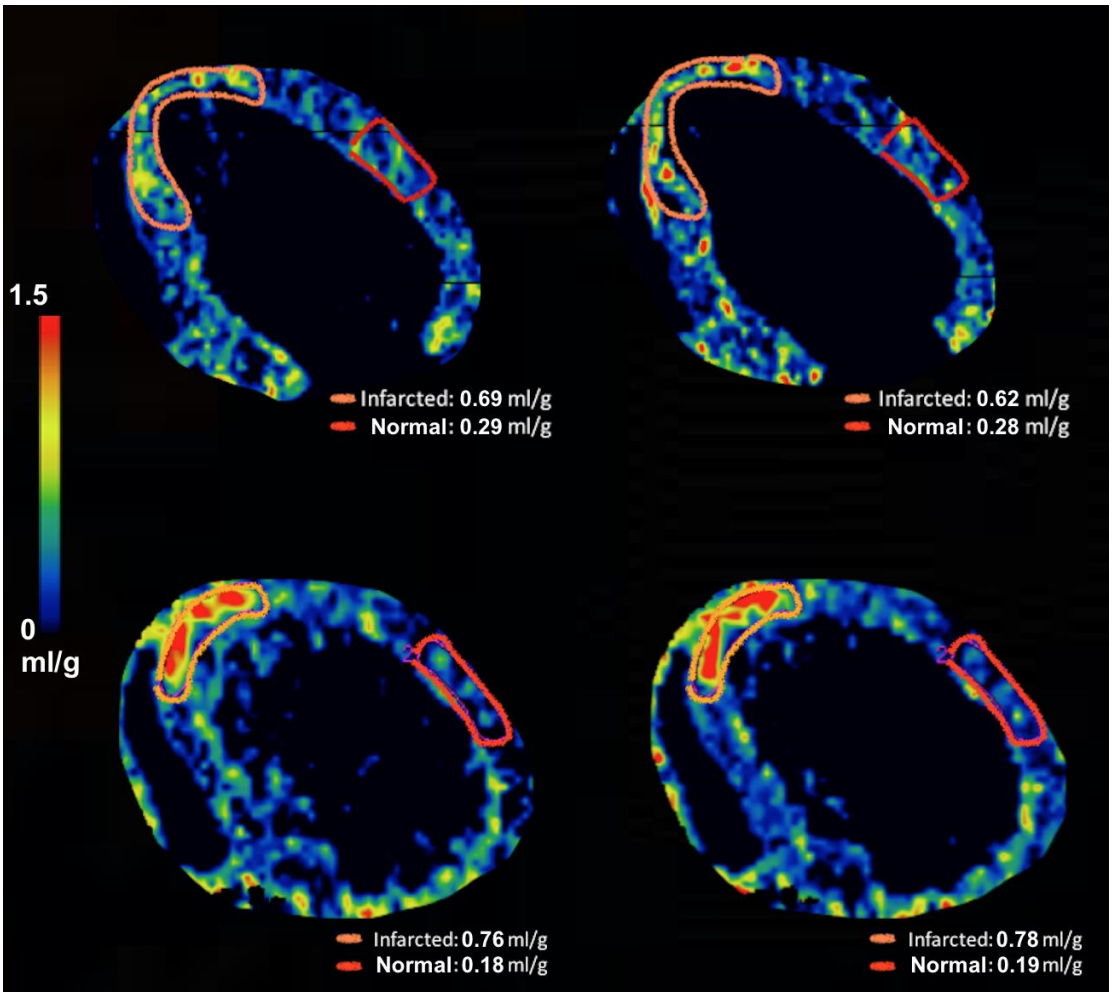

Figure 3-3 ECDV map of a two subjects (top and bottom row) at two different scan durations. ECDV map corresponding to the short scan duration utilizing three phases is shown on the left column and ECDV map corresponding to the long scan duration utilizing four phases is shown on the right column. Infarcted myocardium is denoted in orange and the normal (remote) myocardium is outlined in red.

3.3.3 Potential application of ECDV in sub-acute and chronic MI

For the majority of my thesis work, only data from the acute phase (day 3) post insult were analyzed. The ECDV and MP thresholds were determined for subjects during the acute phase after MI. Previous literature suggests that hemodynamics within the injured tissue change as the heart begins its remodeling process (14,15). A major change that takes place is the resolution of edema and the development of scar tissue. It would be

interesting to test the potentials of ECDV and MP at later phases of MI to monitor the change in area of salvageable myocardium for patients who do not receive treatment within the ideal revascularization treatment window.

With DCE-CT, the change in contrast enhancement of the region of interest can be monitored over time, and the distribution of contrast within the myocardium can be assessed by adopting the JWL model of tracer kinetics. In the case of AMI, this technique takes advantage of the edema and inflammation response after reperfusion. ECDV quantification is a technique that may prove useful in other disease assessments as well, one of which would be scar tissue identification in chronic MI patients.

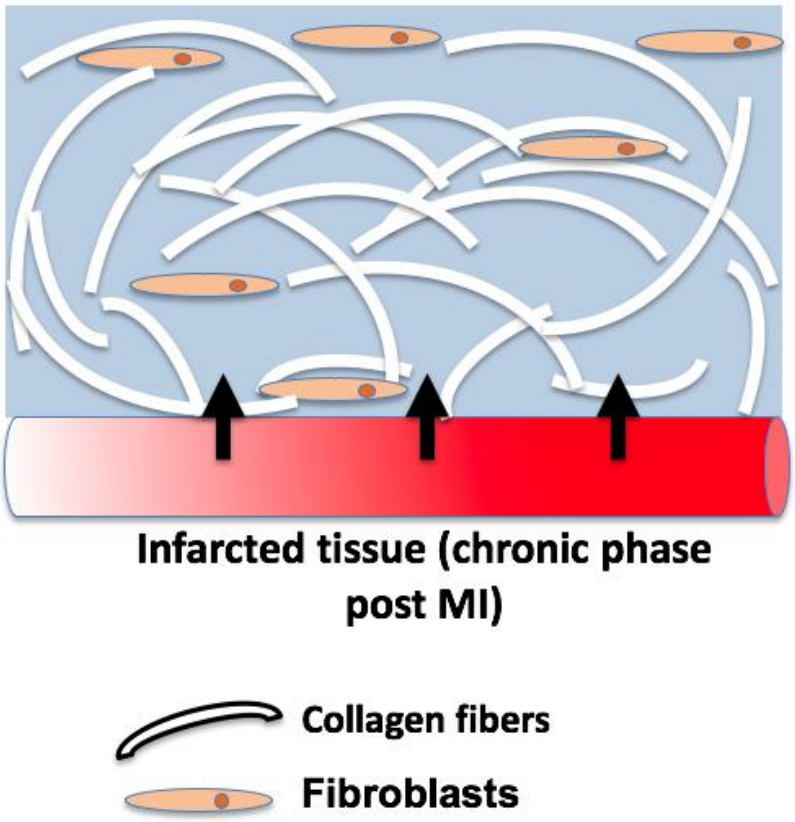

Figure 3-4 Pathophysiology within infarcted myocardium at chronic MI. This figure depicts the development of extracellular matrix composed of high concentration of collagen fiber.

During the chronic end stages of MI, the necrotic myocardium is replaced by collagenous scar tissue—a healing process for the damaged heart (Figure 3-4) (15). The phases leading to heart remodeling were divided into three stages by Richardson and colleagues: inflammation/necrosis, fibrosis, and long-term heart remodeling. Our ECDV technique can take advantage of the space of the extravascular compartment of excessively developed extracellular matrix of scarred myocardium.

Following necrosis, the fibrotic stage can last from one to several weeks depending on the degree of injury. During this phase, myofibroblast increase in abundance accompanied by upregulation of matrix proteins and contractile abilities, specifically in areas of infarcted myocardium. With careful regulations and balance of the above, collagen content effectively increases. A compact extracellular matrix is structured by the cross-link of many collagen fibers. The volume of space in which contrast agents can accumulate is dependent on the density of the collagen fibers of the extracellular matrix. This assumption has been tested using cardiac MR to image scar development at chronic stages of MI.

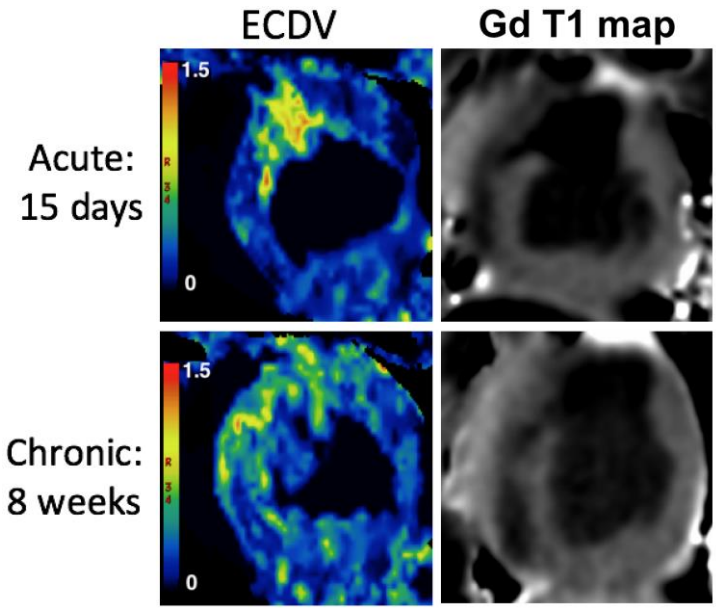

Figure 3-5 ECDV (left) and gadolinium enhanced MR (right) of a subject at acute MI and chronic MI.

Gadolinium enhanced MR for assessment of chronic MI has become an accepted standard in detecting myocardial scar (16-18). Characterization of scar in terms of size and location has proven useful in determining the clinical outcome of patients who have undergone myocardium damage. Preliminary results of a single subject at the acute and chronic phases of MI have demonstrated the potential of ECDV in characterizing chronic MI (Figure 3-5). Figure 3-5 shows enhancement in the injured myocardium region of a subject's heart imaged in short axis view, corresponding to the hypoenhanced area of a gadolinium enhanced T1-map in acute and chronic MI. The retention of contrast that is shown through the ECDV and gadolinium T1 map in acute phase MI is a result of edema; however, the retention of contrast in injured myocardium at chronic phase MI results from the development of fibrotic tissue. Further investigation with greater sample size is required to test the use of ECDV in scar detection during chronic phase MI.

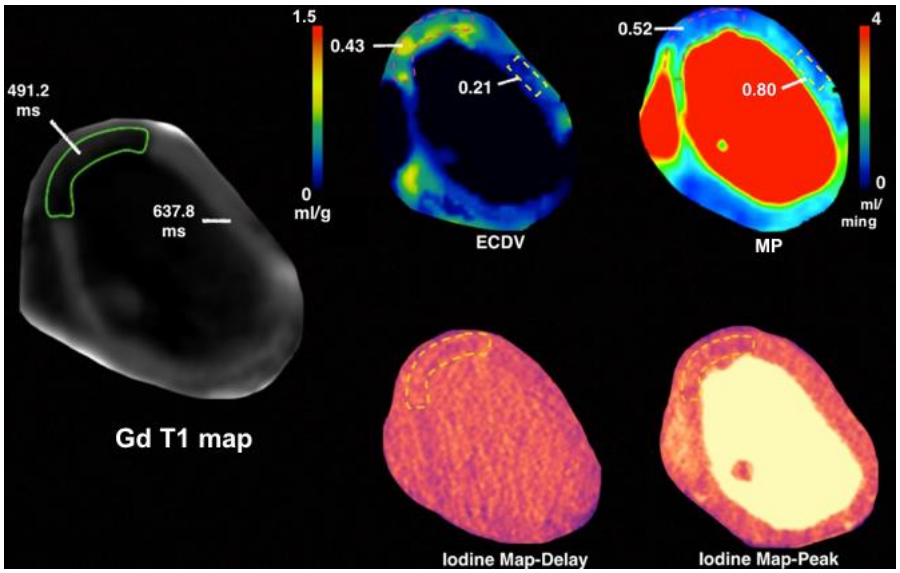

Figure 3-6 CMR Gd enhanced T1 map (left). ECDV and perfusion functional map (top left and right, respectively). Iodine map at delayed phase and at peak contrast enhancement (bottom left and right, respectively).

Another technique used in the clinic for scar detection is iodine mapping using dual energy CT (19). Clinically, iodine mapping has been proposed to assess perfusion after a bolus injection of contrast the hypoenhanced region was delineated on the CMR post gadolinium T1 map representing the region affected by edema. The same region of interest was placed on two iodine maps of the same subject: (1) at peak enhancement of contrast and (2) at

delayed phase of injection (Figure 3-6). The preliminary data suggest that myocardial absolute perfusion measurements and ECDV values obtained from the functional CT technique may be more sensitive and provide quantitative information that may be more valuable compared to the iodine map.

3.3.4 Clinical Translation: triaging patients for revascularization treatment

The clinical motivation of my thesis work is to develop an imaging technique to triage AMI patients for revascularization treatment. Upon patient admission to the hospital, they are subjected to ECG-tracing and blood work as discussed in section 1.1.2. When the patient is diagnosed with STEMI, clinicians can quickly conclude that the patient requires urgent revascularization treatment. In situations where the patient remains asymptomatic with inconclusive ECG and blood work, clinicians can rely on the functional CT technique to estimate ECDV and MP. Quantitative ECDV and MP measurements can then be used to delineate MAR and myocardial salvage. Although the functional CT technique has the potential to be useful in the clinic, guidelines are required to properly triage patients for intervention.

A useful measure for such guidelines is the calculation of the percentage of area that is salvageable myocardium relative to the area of MAR. Once sufficient pre-clinical evidence is acquired, a clinical study should be performed to determine a percentage threshold of percent area of salvage myocardium to area of MAR to identify which patients would most benefit from revascularization treatment.

3.4 References

1. Lee T-Y. Functional CT: physiological model. Trends in Biotechnology 2002;20:S3-S10

2. So A, Wisenberg G, Teefy P et al. Functional CT assessment of extravascular contrast distribution volume and myocardial perfusion in acute myocardial infarction. Int J Cardiol 2018 Sep 1; 266:15-23

3. So A, Hsieh J, Li JY, Hadway J, Kong HF, Lee TY. Quantitative myocardial perfusion measurement using CT perfusion: a validation study in a porcine model of reperfused acute myocardial infarction. Int J Cardiovasc Imaging 2012;28:1237-48.

4. So A, Lee TY. Quantitative myocardial CT perfusion: a pictorial review and the current state of technology development. J Cardiovasc Comput Tomogr 2011;5:467-81.

5. Arbab-Zadeh A, Di Carli MF, Cerci R et al. Accuracy of Computed Tomographic Angiography and Single-Photon Emission Computed Tomography-Acquired Myocardial Perfusion Imaging for the Diagnosis of Coronary Artery Disease. Circ Cardiovasc Imaging 2015;8:e003533.

6. Bamberg F, Marcus RP, Becker A et al. Dynamic myocardial CT perfusion imaging for evaluation of myocardial ischemia as determined by MR imaging. JACC Cardiovasc Imaging 2014;7:267-77.

7. Heo R, Nakazato R, Kalra D, Min JK. Noninvasive imaging in coronary artery disease. Semin Nucl Med 2014;44:398-409.

8. Kitagawa K, Sakuma H, Nagata M et al. Diagnostic accuracy of stress myocardial perfusion MRI and late gadolinium-enhanced MRI for detecting flow-limiting coronary artery disease: a multicenter study. Eur Radiol 2008;18:2808-16.

9. Ko SM, Choi JW, Song MG et al. Myocardial perfusion imaging using adenosine-induced stress dual-energy computed tomography of the heart: comparison with cardiac magnetic resonance imaging and conventional coronary angiography. Eur Radiol 2011;21:26-35.

10. Rochitte CE, George RT, Chen MY et al. Computed tomography angiography and perfusion to assess coronary artery stenosis causing perfusion defects by single photon emission computed tomography: the CORE320 study. Eur Heart J 2014;35:1120-30.

11. Varga-Szemes A, Meinel FG, De Cecco CN, Fuller SR, Bayer RR, 2nd, Schoepf UJ. CT myocardial perfusion imaging. AJR Am J Roentgenol 2015;204:487-97.

12. Bandula S, White S, Flett AS et al. Measurement of Myocardial Extracellular Volume Fraction by Using Equilibrium Contrast-enhanced CT: Validation against Histologic Findings. Radiology 2013;269.

13. Mahnken AH, Bruners P, Bornikoel CM, Kramer N, Guenther RW. Assessment of myocardial edema by computed tomography in myocardial infarction. JACC Cardiovasc Imaging 2009;2:1167-74.

14. Walls MC, Verhaert D, Min JK, Raman SV. Myocardial edema imaging in acute coronary syndromes. J Magn Reson Imaging 2011;34:1243-50.

15. Richardson WJ, Clarke SA, Quinn TA, Holmes JW. Physiological Implications of Myocardial Scar Structure. Compr Physiol 2015;5:1877-909.

16. Truong QA, Thai WE, Wai B et al. Myocardial scar imaging by standard single-energy and dual-energy late enhancement CT: Comparison with pathology and electroanatomic map in an experimental chronic infarct porcine model. J Cardiovasc Comput Tomogr 2015;9:313-20.

17. McAlindon E, Pufulete M, Lawton C, Angelini GD, Bucciarelli-Ducci C. Quantification of infarct size and myocardium at risk: evaluation of different techniques and its implications. Eur Heart J Cardiovasc Imaging 2015;16:738-46.

18. Tanabe Y, Kido T, Kurata A et al. Late iodine enhancement computed tomography with image subtraction for assessment of myocardial infarction. Eur Radiol 2018;28:1285-1292.

19. Wichmann JL, Bauer RW, Doss M et al. Dianostic Accuracy of Late Iodine-Enhancement Dual-Enegy Computed Tomography for the Detection of Chronic Myocardial Infarction Compared With Late Gadolinium-Enhancement 3-T Magnetic Resonance Imaging. Investigative Radiology 2013;48:851-856.

Appendices

Appendix A: Quality of ECDV functional maps using full scan and partial scan retrospective reconstruction

The previously published paper adopted the use of full-scan reconstruction (1). However, retrospective evaluation of the time enhancement curves indicated large variability in measured average enhancement at the later time points (phases 2 and 3 of the acquisition); see Figure A-1. This observation was consistent with observations made during the acquisition where, near the end of the four-minute dynamic scan, subjects were “fighting” against the manual breath-hold via ventilator. To reduce the effect of motion during acquisition, the same set of raw DCE-CT projection data were retrospectively reconstructed to produce partial-scan images for each of the seven subjects at the acute phase. As describe in Chapter 2, images were averaged to produce 5-mm thick slices and the dynamic scan images were registered to each other to minimize motion artifact during the single dynamic imaging session (as per the full scan reconstructed images). ECDV and MP functional maps were generated (Figure A-1) using the extended JWL tracer kinetics model and the values within the myocardial regions defined in Chapter 2 were calculated. Analysis was performed only on the ECDV data.

Qualitatively, Figure A-1 shows greater difference between injured and normal myocardium is seen in the ECDV maps derived from the partial scan reconstruction than the full scan reconstruction. Quantitative comparison of the ECDV values in the apical septal (injured) and mid-lateral (normal) walls of the myocardium obtained from the full and partial scan are shown in Figure A-2. The figure shows greater difference in ECDV between infarcted and normal myocardium when partial scan reconstruction is used ($p< 0.0001$) vs. full-scan reconstruction ($p<0.05$). Therefore, partial scan reconstruction was utilized for the all data presented in this thesis.

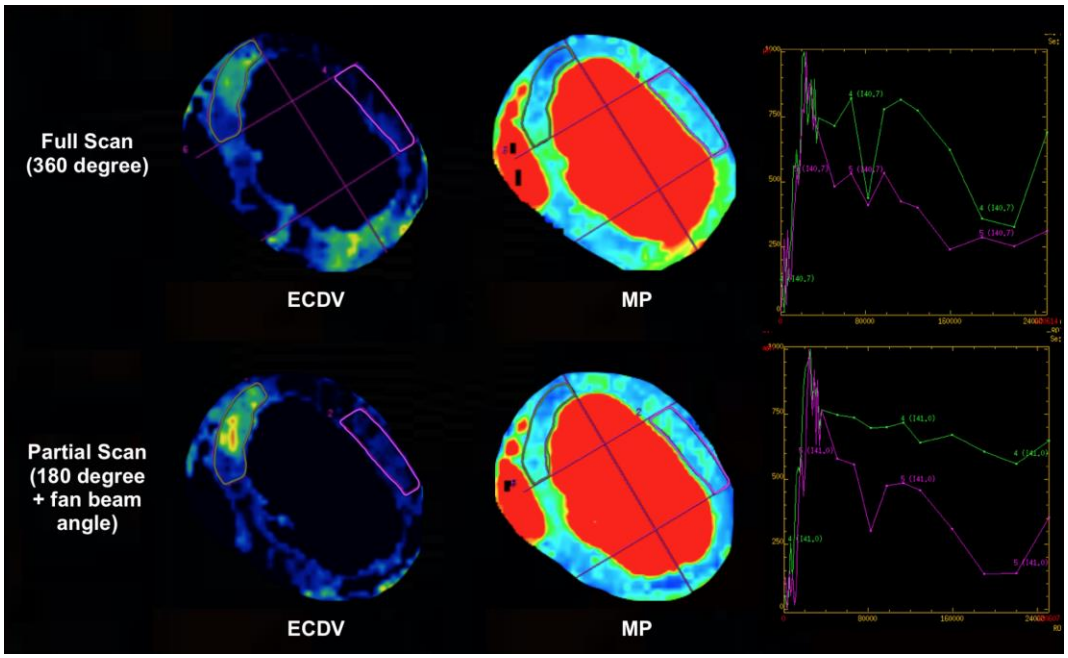

Figure A-1 ECDV and MP maps of a subject using full scan and partial scan reconstruction. Graphs on the right illustrate the normalized time enhancement curves of the injured apical septal wall (green) and normal mid-lateral myocardium (purple). ECDV scale 0 to 1.2 ml/g and MP scale from 0 to 5.0 ml/min/g.

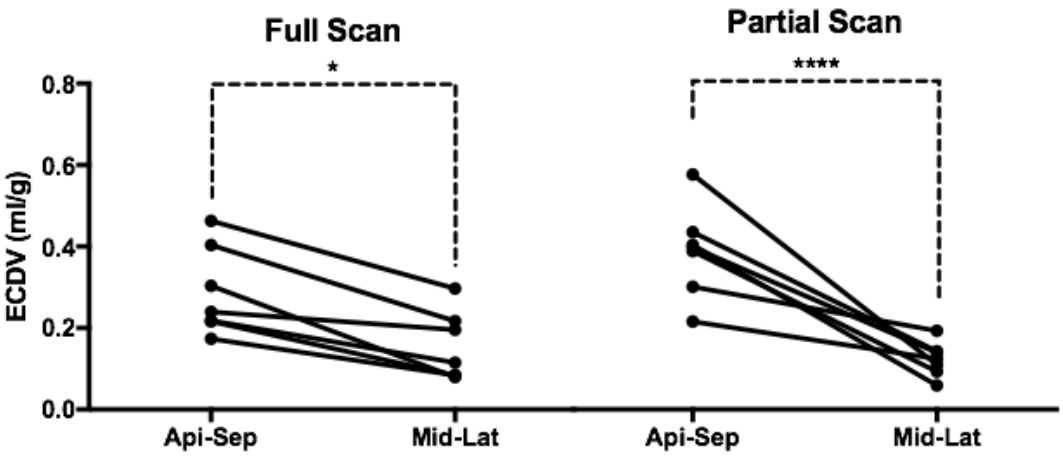

Figure A-2 ECDV (ml/g) of infarct and normal myocardium for each subject compared using full scan and partial scan reconstruction. (* denote $p < 0.05$, **** denote $p < 0.0001$).

Reference

1. So A, Wisenberg G, Teefy P et al. Functional CT assessment of extravascular contrast distribution volume and myocardial perfusion in acute myocardial infarction. Int J Cardiol 2018 Sep 1;266:15-23

Appendix B: Institution Research Ethics Board Approval

Western

Dec.. 23 , 2009

This is the Original Approval for this protocol
A Full Protocol submission will be required in 2013

Dear Dr. Lee:

Your Animal Use Protocol form entitled:
CT and PET Imaging of Normal Myocardium
Funding Agency ORF ICT - Grant #LRI 7768506

has been approved by the University Council on Animal Care. This approval is valid from **December 23, 2009 to December 31, 2010.** The protocol number for this project is **#2009-092**.

1. This number must be indicated when ordering animals for this project.
2. Animals for other projects may not be ordered under this number.
3. If no number appears please contact this office when grant approval is received.
   If the application for funding is not successful and you wish to proceed with the project, request that an internal scientific peer review be performed by the Animal Use Subcommittee office.
4. Purchases of animals other than through this system must be cleared through the ACVS office. Health certificates will be required.

ANIMALS APPROVED FOR 4 Years

SPECIES & SECT D.5.1 GROUP ID#	STRAIN &/or OTHER SPECIES DETAIL For Rodents, Also Provide Vendor Stock #	AGE or WEIGHT & SEX	4-YEAR TOTAL ANIMAL NUMBER
Pig ID# all	Farm pig	15-25 kg Female	32

REQUIREMENTS/COMMENTS
Please ensure that individual(s) performing procedures on live animals, as described in this protocol, are familiar with the contents of this document.
The holder of this Animal Use Protocol is responsible to ensure that all associated safety components (biosafety, radiation safety, general laboratory safety) comply with institutional safety standards and have received all necessary approvals. Please consult directly with your institutional safety officers.

c.c. Approved Protocol - T. Lee, J. Hadway, D. Forder
Approval Letter - T. Lee, J. Hadway, D. Forder

***The* University *of* Western Ontario**
Animal Use Subcommittee / University Council on Animal Care
Health Sciences Centre, • London, Ontario • CANADA – N6A 5C1
PH: 519-661-2111 ext. 86770 • FL 519-661-2028 • www.uwo.ca / animal

Curriculum Vitae

Name:	Lisa Yun Jeong Hur
Post-secondary Education and Degrees:	**Master of Science** Medical Biophysics University of Western Ontario London, Ontario, Canada September 2016 – August 2018 **Bachelor of Science** Major in Botany The University of Calgary Calgary, Alberta, Canada September 2012 – April 2016
Honours and Awards:	**Western Graduate Research Scholarship** Department of Medical Biophysics. University of Western Ontario 2017-2018
Related Work Experience	**Research Assistant** The University of Calgary Calgary Stroke Program 2013-2016 **Research Assistant** The University of Calgary Hotchkiss Brain Institute 2013-2015
Publications:	Najm M, Al-Ajlan FS, Boesen ME et al. Defining CT Perfusion Thresholds for Infarction in the Golden Hour and With Ultra-Early Reperfusion. Can J Neurol Sci 2018;45:339-342. Batchelor C, Pordeli P, d'Esterre CD et al. Use of Noncontrast Computed Tomography and Computed Tomographic Perfusion in Predicting Intracerebral Hemorrhage After Intravenous Alteplase Therapy. Stroke 2017;48:1548-1553.
Oral Presentation:	**Hur L**, Wisenberg G, Teefy P et al. Quantitative CT assessment of myocardial edema in acute myocardial infarction: a validation study. Radiological Society of North America Annual Meeting 2017, Chicago, Illinois, USA, November 27, 2017

Hur L, Wisenberg G, Teefy P et al. Quantitative CT assessment of myocardial edema in acute myocardial infarction: a validation study. Imaging Network of Ontario 2017, London, Ontario, Canada, March 15, 2017

Poster Presentation: **Hur L**, Wisenberg G, Teefy P et al. A Single Bolus Injection of Contrast in Quantitatively Assessing Myocardial Edema: A Validation Study. London Health Research Day 2017, London, Ontario, Canada, March 28, 2017